Revisiting the tropical Atlantic western boundary circulation from a 25-year time series of satellite altimetry data

Djoirka M. Dimoune[1,4], Florence Birol[2], Fabrice Hernandez[1,2], Fabien Léger[2], Moacyr Araujo[1,3]

[1]Laboratorio de Oceanografia Física Estuarina e Costeira (LOFEC), Departamento de Oceanografia da Universidade Federal de Pernambuco (UFPE), Cidade Universitária, Avenida Arquitetura s/n, 50740-550 Recife, PE, Brazil

[2]LEGOS, Université de Toulouse, CNES, CNRS, IRD, 14~~8~~ avenue Edouard Belin, 31400, France

[3]Brazilian Research Network on Global Climate Change (Rede CLIMA), Av. dos Astronautas, 1758, 01227-010 São José dos Campos, SP, Brazil

[4]Nansen Tutu Center for Marine Environmental Research, Dept of Oceanography, University of Cape Town, Rondebosch, Cape Town, 7700, South Africa

Correspondance to: Djoirka M. Dimoune (pmintodimoune@gmail.com)

Abstract. Geostrophic currents derived from altimetry are used to investigate the surface circulation in the Western Tropical Atlantic over the 199~~3~~8-2017 period. Using six horizontal sections defined to capture the current branches of the study area, we investigate their respective variations at both seasonal and interannual time-scales as well as the spatial distribution of these variations in order to highlight the singularities of the currents on their route. Our results show that the central branch of the South Equatorial Current, its northern branch near the Brazilian coast, the North Brazil Current component located south of the equator and~~,~~ the Guyana Current ~~and the northern branch of the South Equatorial Current at 42° W~~ have similar annual cycles, with maxima/minima respectively, during late boreal winter ~~spring~~/boreal fall~~October-November~~ when the Intertropical Convergence Zone is at its southernmost/northern location. In contrast, the seasonal cycles of the North Brazil Current branch located between the equator and 7-8° N, its~~the North Brazil Current~~ retroflected branch, the northern branch of the South Equatorial Current to the west of 35° W and the North Equatorial Countercurrent show maxima/minima during late boreal summer~~fall~~/boreal spring~~May~~ following the remote wind stress curl strength variation. West of 3~~4~~2° W, an eastward current is observed between 0°-2° N, identified as the equatorial extension of the retroflected branch of the North Brazil Current. It is part of a large cyclonic circulation observed between 0°-6° N and 35°-45° W during boreal spring. ~~The North Equatorial Countercurrent shows a two-core structure during the second half of the year, when we~~We also observed ~~the two regions where the~~a secondary North Brazil Current retroflect~~ions~~ flow during the second half of the year which leads to the two-core structure of the North Equatorial Countercurrent, and might be related to the wind stress curl

seasonal changes. Eastward, the North Equatorial Countercurrent weakens and its two-core structure is underdeveloped due to the weakening of the wind stress~~The latter can be related to the wind stress curl seasonal changes~~. At interannual scales, depending on which side of the equator, the North Brazil Current exhibits two opposite scenarios related to the tropical Atlantic Meridional Mode phases. The interannual variability of the North Equatorial Countercurrent and of the northern branch of the South Equatorial Current (in terms of both strength and/or latitudinal shift) at 42° W are also associated to the Atlantic Meridional Mode. However,~~, while~~ they are associated to the Atlantic~~zonal~~ mode phases at 32° W.

1   Introduction

The energetic Western Tropical Atlantic (WTA) boundary surface circulation is known to play a key role in the transport of heat, salt and water mass from the southern to the northern hemispheres of the Atlantic Ocean. It corresponds to a superposition of the return branch of the thermohaline Atlantic Meridional Overturning Circulation (AMOC), the flow from the Subtropical Cells and Sverdrup dynamics~~influenced by the wind~~ (Schmitz and McCartney, 1993; Schott et al., 2004, 2005; Rodrigues et al., 2007, Tuchen et al., 2019, 2020). The region is also known to be influenced by large mesoscale activities due to the barotropic instabilities of the currents. The most dominant mesoscale structures are the large rings generated by North Brazilian Current (NBC) retroflection (Aguedjou et al., 2019; Aroucha et al., 2020). A regional scheme of the surface currents in the study area is proposed in Fig. 1. It is derived from a global analysis of the different studies~~works~~ mentioned hereafter~~below~~.

From 5° S to 15° N, the surface boundary circulation is formed by the ~~North Brazil Current (~~NBC~~)~~ flowing northward along the South American shelf. It carries tropical waters originating from the South Atlantic subtropical gyre and contributes to interhemispheric water transport (Johns et al., 1990; 1998; Peterson and Stramma, 1991; Stramma and England, 1999; Fratantoni et al., 2000; Silva et al., 2009; Zheng and Giese, 2009~~;~~, Garzoli and Matano, 2011). The NBC has its origin near 5° S, with two sources: the central branch of the westward South Equatorial Current (cSEC); and the along-shelf equatorward North Brazil Undercurrent (NBUC) which ~~rises to the ~~surfaces around 5-6° S (Schott et al., 1998, Dossa et al., 2020). The latter advects warm waters from the South Equatorial Current (SEC) through its southern branch (Schott et al., 1995). Further north, around 5° N, the NBC is also fed by the northern branch of the SEC (nSEC) (Goes et al., 2005). Then, between 5°-9° N and 45-50° W, a large part of the NBC

68 retroflects to form a southeastward retroflected branch (called hereinafter rNBC). Between 3°
69 N and 8° N, this branch first feeds the eastward North Equatorial Countercurrent (NECC)
70 throughout the year, except during the boreal spring. At that time, the NECC is fed only by the
71 North Equatorial Ceurrent (NEC) (Bourlès et al., 1999a; Goes et al., 2005). The NECC flows
72 eastward between 2° N and 12° N, and crosses the tropical Atlantic (Didden and Schott, 1992;
73 Ffield, 2005; Urbano et al., 2008; Araujo et al., 2017). During the second half of the year, this
74 current shows two cores that can separate into a southern and a northern branch (called sNECC
75 and nNECC, respectively: Urbano et al., 2006; 2008).

76 At depth, around 3-8° N, Cochrane et al. (1979) and Schott et al. (2004) suggested that, part of
77 the rNBC also feeds the eastward North Equatorial UnderCurrent (NEUC) located around 5°
78 N. In addition, between 2° S and 3° N, the rNBC feeds the subsurface eastward Equatorial
79 UnderCurrent (EUC) (Hisard and Hénin, 1987; Bourlès et al., 1999b; Hazeleger et al., 2003;
80 Hazeleger et de Vries, 2003; Schott et al., 1995; 2004). North of 10° N, the part of the NBC
81 which has not retroflected flows northwestward along the Guyana coast, forming the Guyana
82 Current. The latter is also fed seasonally by the NEC (Johns et al., 1998) and transports warm
83 equatorial waters into the Caribbean Sea (Stramma and Schott, 1999; Garzoli et al., 2003).

84 The WTA boundary surface circulation is wind-driven. In the vorticity equation, the terms that
85 dominate localy are the Ekman pumping and the divergence of the geostrophic currents (Garzoli
86 and Katz, 1983; Urbano et al., 2006). ~~The region is also known to be influenced by large~~
87 ~~mesoscale activities due to the barotropic instabilities of the currents (Aguedjou et al., 2019;~~
88 ~~Aroucha et al., 2020).~~ Previous studies of Garzoli and Katz (1983), Jochum and Malanotte-
89 Rizzoli (2003) and Verdy and Jochum (2005) about the WTA boundary circulation and the
90 NECC indicate that, west of 32° W, the Sverdrup balance is no longer satisfied~~more respected~~;
91 the advection terms of the relative vorticity due to the eddies and the mean flow become then
92 important. North of the equator, the region is characterized by strong seasonal variability of the
93 wind. The Trade Winds variations influence the current system formed by the NBC, the NBC
94 retroflection (NBCR), the rNBC and the NECC. In particular the NBCR location, the NBC
95 transport and the NECC position/transport respond to the seasonal changes in the wind regimes
96 (Johns et al., 1990; 1998; Garzoli et al., 2003; 2004; Urbano et al., 2006; 2008). This wind
97 influence is traduced by ~~a~~ latitudinal shifts~~changes~~ of the currents, in conjunction with the
98 Intertropical Convergence Zone (ITCZ) location. The variability of the current strength appears
99 as a regional response to~~of~~ the wind stress curl (WSC) distribution and of the WSC strength
100 over the basin (Johns et al., 1998; Fonseca et al., 2004; Garzoli et al., 2004, Urbano et al., 2006;

101 2008). In the equatorial region, the EUC seasonal variability depends~~is~~ first on~~associated to~~ the

102 basic scale zonal pressure gradient ~~(ZPG)~~, and also to the seasonal cycle of the local wind

103 forcing (Hisard and Hénin, 1987; Provost et al., 2004; Brandt et al., 2006; Hormann and Brandt,

104 2007; Brandt et al., 2016).

105 The interannual variability of the WTA boundary currents has been under~~little~~ studied because

106 of the lack of long-term data in this area. Nevertheless, Fonseca et al. (2004), using a

107 combination of altimetry and hydrographic data from 1993 to 2000, investigated the influence

108 of the wind on both the NBCR and the NECC variability. They did not find any direct

109 relationship between them. Hormann et al. (2012), used the surface velocity data derived from

110 drifters between 1993 and 2009 and highlighted a relationship between the NECC

111 intensity/location and the tropical Atlantic climate modes (ACM), represented by positive and

112 negative phases of the Atlantic zonal mode (AZM) and the Atlantic meridional mode (AMM)

113 (Cabos et al., 2019). They found the intensity to be related to the cold phase of AZM and the

114 core location to be related to the warm phase of AMM. In the equatorial Atlantic, Hormann and

115 Brandt (2007) also found such relationship, using a high-resolution ocean general circulation

116 model, observations and sea surface temperature (SST) data. They showed that the EUC

117 transport is affected by the cold and warm events of the AZM (the so called "Atlantic Niño /

118 Niña") and confirmed the previous findings of Goes and Wainer (2003) concerning the link

119 between the interannual variability of the wind and the ACM impacting the strength of the

120 tropical Atlantic circulation.

121 In this study, we propose to revisit the scheme of the WTA boundary surface circulation using

122 a 25-year time series of gridded altimeter-derived geostrophic currents. This dataset is longer

123 than the one used by Fonseca et al. (2004) and allows us to provide a more robust description

124 of the current branches described above, as well as of their seasonal and interannual variations.

125 The data also allows us to infer regional relationship among these currents. The paper is

126 organized as follows: in Sect. 2, the data and methods used are presented. Section 3 brings some

127 general characteristics of the current variability in the study area. In the fourth section we

128 analyze and discuss the seasonal and spatial variabilities of the surface geostrophic currents and

129 propose an updated seasonal map of the WTA surface circulation. The interannual variability

130 of the circulation is analyzed in Sect. 5. Section 6 is devoted to a general discussion, and Sect.

131 7 offers a summary and some perspectives.

132

133

134

135

136

137
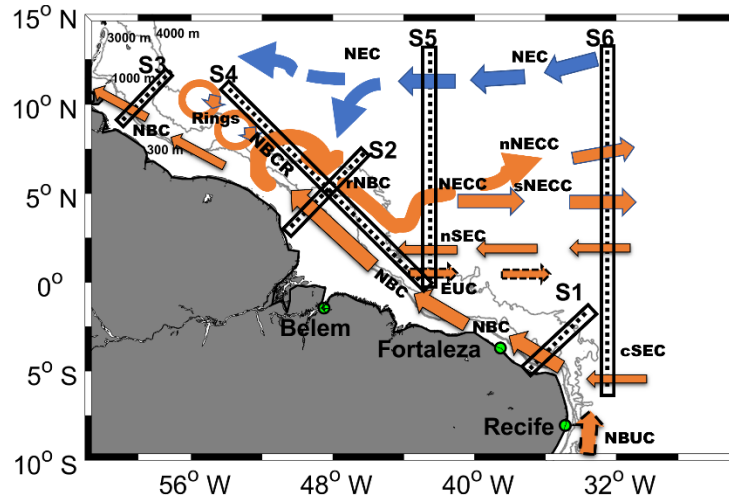
Figure 1. Schematic view of the western boundary surface circulation in the tropical Atlantic ~~based on~~derived ~~from~~ Schott et al. (2004), Goëes et al. (2005), Urbano et al. (2006; 2008) and Aroucha et al. (2019). The distribution of the horizontal section used to study the different current branches are also indicated in black: S1, S2, S3, S4, S5 and S6. Solid and dashed arrows are the upper and the subsurface currents, respectively. The blue and orange colors of the arrows show connections with the northern and southern hemisphere waters, respectively. Acronyms are listed in Table 1. ~~From south to north, the currents shown are the North Brazil Undercurrent (NBUC), the central and northern branches of the South Equatorial Current (cSEC and nSEC, respectively), the North Brazil Current, its retroflection and its retroflected branch (NBC, NBCR and rNBC, respectively), the Equatorial Undercurrent (EUC), the North Equatorial Countercurrent (NECC) and its southern and northern branches (sNECC and nNECC, respectively), and the North Equatorial Current (NEC).~~ The 300 m, 1000 m, 3000 m and 4000 m isobaths (grey lines) are from the ETOPO2v1 database.

150

151

152

153

154

155

156

157

158

159

160

161

162

2   Data and methods

2.1   Altimeter-derived geostrophic currents

From along-track altimetry sea surface height measurements of all available satellite missions, the Copernicus Marine Environment Monitoring Service (CMEMS) produces daily maps of ocean dynamic topography, and derives then geostrophic surface currents. Here, we use the SEALEVEL_GLO_PHY_L4_REP_OBSERVATIONS_008_047 product (https://resources.marine.copernicus.euhttps://resources.marine.copernicus.eu/) from January 1993 to December 2017. Daily maps of dynamic topography are estimated by optimal interpolation on $0.25° \times 0.25°$ global grid (details can be found in Pujol et al., 2016), and the geostrophic currents are computed using the 9-points stencil width methodology (Arbic et al., 2012) for latitudes outside the equatorial band (Equator $\pm5°$) and the β-plane approximation in the equatorial band, the currents have been calculated using the Lagerloef methodology (Lagerloef et al., 1999) which used a β-plane approximation due to the fact that the Coriolis parameter is vanishing.

To validate geostrophic current estimates in the equatorial region, we have compared them to the PIRATA current meter mooring data available in the study area (0°N, 35°W) over the 11/10/2017-29/01/2018 (Fig. 1 in the supplementary material). The data of the current meter were obtained at 12-m depth and have been averaged each 5 days. The results of the comparison with the geostrophic currents interpolated to the same location were satisfactory. A correlation of 0.71 is found on their zonal components while the one on the meridional components is lower (Figure 1a-b in the supplementary material). The mean biases/standard deviation differences for both components are respectively, 0.04/0.11 m s^{-1} and 0.14/0.03 m s^{-1}. The similar values were also found by Lagerloef et al. (1999) in the western equatorial Pacific when comparing the geostrophic currents to the current meter mooring data at 10-m depth. These results give credit to the geostrophic estimates used in this work for the equatorial region. However, as reported earlier, their values are underestimated compared to other observations (Picaut et al.,

1989; Lagerloef et al., 1999, Pujol et al., 2016). The PIRATA 0-35°W current meter was also able to capture an eastward flow at this location from November 2018 to March 2019. This confirms the previous findings of the Bourlès et al. (2019) and legitimizes our desire to know more about this flow.

Table 1. Acronyms and abbreviations

AMM	Atlantic Meridional Mode
AMOC	Atlantic Meridional Overturning Circulation
AZM	Atlantic Zonal Mode
EUC	Equatorial Undercurrent
ITCZ	Intertropical Convergence Zone
NBC	North Brazil Current
rNBC	Retroflected branch of the NBC
NBCR	North Brazil Current Retroflection
nNBCR	Northern NBCR flow
nNBCR_lat	Latitude of the nNBCR maximum intensity
sNBCR	Southern NBCR flow
sNBCR_lat	Latitude of the sNBCR maximum intensity
NECC	North Equatorial Countercurrent
nNECC	Northern branch of the NECC
nNECC_lat	Latitude of the nNECC core
sNECC	Southern branch of the NECC
sNECC_lat	Latitude of the sNECC core
PIRATA	Prediction and Research Moored Array in the Tropical Atlantic
SEC	South Equatorial Current
cSEC	Central branch ot the SEC
nSEC	Northern branch of the SEC
VnNBCR	Value of the nNBCR maximum speed
VsNBCR	Value of the sNBCR maximum speed
VnNECC	Value of the nNECC core speed
VsNECC	Value of the sNECC core speed
X	Equatorial Surface Eastward flow
WSC	Wind Stress Curl
WSC neg max	Maximum negative WSC
WSC strength	WSC strength
WTA	Western tropical Atlantic

For the present work, focusing on the seasonal and interannual variability, the daily gridded velocity fields from CMEMS have been averaged ~~on a~~ monthly ~~basis~~. Note that, data with high variability (standard deviation > 0.4) have been removed. They are found in the Amazon region which is not a primary area of interest for this study, and where, the annual mean current speeds are unrealistic (higher than 2.5 m s^{-1}), probably due to geographically correlated errors (Pujol et al., 2016). ~~we have removed data located in the Amazon region because they show unrealistic values, probably due to erroneous altimetry measurements which have not been correctly flagged.~~ We have then defined six horizontal sections (called S1, S2, S3, S4, S5 and S6,

respectively), so that they cross perpendicularly at least one of the regional current branches (see Fig. 1). For each section, the original zonal and meridional surface velocity components have been rotated in order to derive the along-section and cross-section velocity components. In this study, we considered only the cross-section component, and the rotation angles considered for the oblique sections S1-S2-S3/S4 are 45°/315°.

2.2 Ekman currents

We also used the GEKCO product (Geostrophic and Ekman Current Observatory, Sudre et al., 2013), made available by LEGOS (Laboratoire d'Etudes en Géophysique et Océanographie Spatiale). It provides the zonal and meridional components of the daily wind driven currents at a 0.25° resolution. The latter were calculated using the standard Ekman formulation, and the estimates have been improved in the equatorial region. Then, they were validated with independent observations from both Lagragian and Eulerienne perspectives (see Sudre et al. 2013 for more details). For this work, the daily current estimates have been monthly averaged over the period 1993-2017.

2.32.2 Wind velocity

Monthly wind velocity fields from the ERA5 atmospheric reanalysis produced by the European Centre for Medium-Range Weather Forecasts (ECMWF, http://www.ecmwf.int) are used in order to evaluate the influence of the remote winds on the WTA ocean circulation. They were downloaded from the Copernicus Climate Change data server over the January 1993 - December 2017 period. We used the wind velocity data to calculate the wind stress field as follows.

The zonal and meridional components of the wind stress, ζ_x and ζ_y are calculated using empirical formulations (Large and Pound; 1981: Gill, 1982; Trenberth et al., 1990) following NRSC (2013):

$$\tau\zeta_x=\rho_{air}C_DW*U \qquad (1)$$

$$\tau\zeta_y=\rho_{air}C_DW*V \qquad (2)$$

where U/V represent the zonal/meridional wind velocity components; W, the wind speed amplitude; ρ_{air}, the air density (1.2 kg m^{-2}); C_D, the drag coefficient at the ocean surface, calculated according to Large and Pound (1981).

The wind stress curl (WSC) is then deduced following Gill (1982):

234

$$Curl(\zeta) = \frac{\partial\,\zeta y}{\partial x} - \frac{d\zeta x}{dy} \quad Curl(\tau) = \frac{\partial \tau_y}{\partial x} - \frac{\partial \tau_x}{\partial y} \qquad (3)$$

236

Over the tropical Atlantic, fFrom the WSC near-zero valuesestimates, we compute the ITCZ locations have been determined (~zero values location)., Then, the minimum/maximum of the negative/positive WSC values has been found, and the WSC strength values (sum of the absolute minimum negative value and the absolute maximum positive values) have been computedin the tropical Atlantic. Each of these parameters is zonally averaged over the region covering 6° S -16° N, and 30° W-0° EW, following Fonseca et al. (2004).

2.42.3 Sea Surface temperature

Monthly estimates of Sea Surface temperature (SST) are also used in order to compute the Atlantic climate mode indexes and evaluate their possible relationship with the interannual changes observed in the WTA boundary circulation. A global gridded SST product, with a 1° spatial resolution is downloaded from the NOAA repository (https://www.esrl.noaa.gov/psd/data/gridded/data.noaa.oisst.v2.html, Reynolds et al. 2002). The AZM index is calculated considering the SST anomalies (SSTA) relative to the 1993-2017 monthly climatology in the ATL3 region bounded by 3° S-3° N/20° W-0° E (Zebiak, 1993, Hormann et al., 2012). The AMM index is also based on SSTA relative to the 1993-2017 monthly climatology, and calculated as the difference between the spatial average SSTA in the box 5° N-25° N/60° W-20° W and the spatial average SSTA in the box 20° S-5° N/30° W-10° E (Servain, 1991; Hormann et al., 2012).

3 General characteristics of the circulation in the Western Tropical Atlantic

The mean WTA surface geostrophic circulation is first derived by averaging the gridded altimetry current maps over 1993-2017 (Fig. 2a). We distinguish three different areas. From south/east to north/west:

1) The NBC formation area starting around 5°S: the westward cSEC flowing north of 6°S (mean value of ~ 0.3 m s^{-1}) feeds the NBC-NBUC current system around 34°-36° W. The NBC amplitude increases along its northward along-shelf course, up to 0.8 m s^{-1} around 3° S. Then it slows down toward the equator, before increasing again north of

263   3° N. Along the ~~Guyana~~ coast, farther north, its mean velocities are again weaker, with

264   values of ~ 0.3 m s^{-1}.

265   2) The NBC retroflection region between 5°-8° N: in this area, the NBC undergoes an

266   eastward recirculation, which feeds a southeastward path~~vein~~ of current so-called the

267   NBC retroflected branch (rNBC). The rNBC reaches annual mean velocities of ~0.6 m

268   s^{-1}.

269   3) The area located between 3°-6° N and 42°-46° W: it represents the region where the

270   rNBC meanders with an annual mean velocity of 0.5 m s^{-1} to partly feed the surface

271   eastward NECC which decays along its course. This area is located in the region of high

272   wind variability (Figure not shown).

273 In addition, we also observe the westward nSEC flowing between 2°-6° N, with stronger

274 velocity values at the eastern part of the basin (mean velocity larger than 0.3 m s^{-1}).

275 We computed the mean power spectral density of the daily geostrophic current time series in

276 order to detect the dominant components of the WTA current variations (not shown). It

277 highlighted three main energy zones:

278   1) at intraseasonal scales with different peaks at periods less than 120 days,

279   2) at seasonal scale,

280   3) at interannual timescale, with peaks at periods larger than 600 days.

281 We filtered the velocity time series using different cutoff frequencies in order to isolate each of

282 this component of the current variability: below 120 days, between 120 days and 600 days and

283 above 600 days. Then, we computed the ratio between the standard deviation of each filtered

284 current field and of the total current field. The resulting maps (Fig. 2b-d) show the relative

285 importance of each component with regard to the total variance, as a function of the location.

286 We observe the predominance of the seasonal variability in the whole WTA (overall ratio of

287 0.44), with the highest values (0.48) observed along the continental shelf, in the NBC region,

288 and between 0°-2° S east of 36° W. Intraseasonal fluctuations are also important in the same

289 areas (with largest ratio of 0.44) while the interannual variability is ~~only~~ weaker ~~noticeable~~ and

290 the highest values (>0.2) are found in the NECC area north/east of 4° N/40° W ~~, where the~~

291 ~~NECC is located, with values representing less than 0.2 of the total variance~~ (consistent with

292 Richardson and Walsh, 1986). In this study, we focus on the seasonal and interannual

293 timescales.
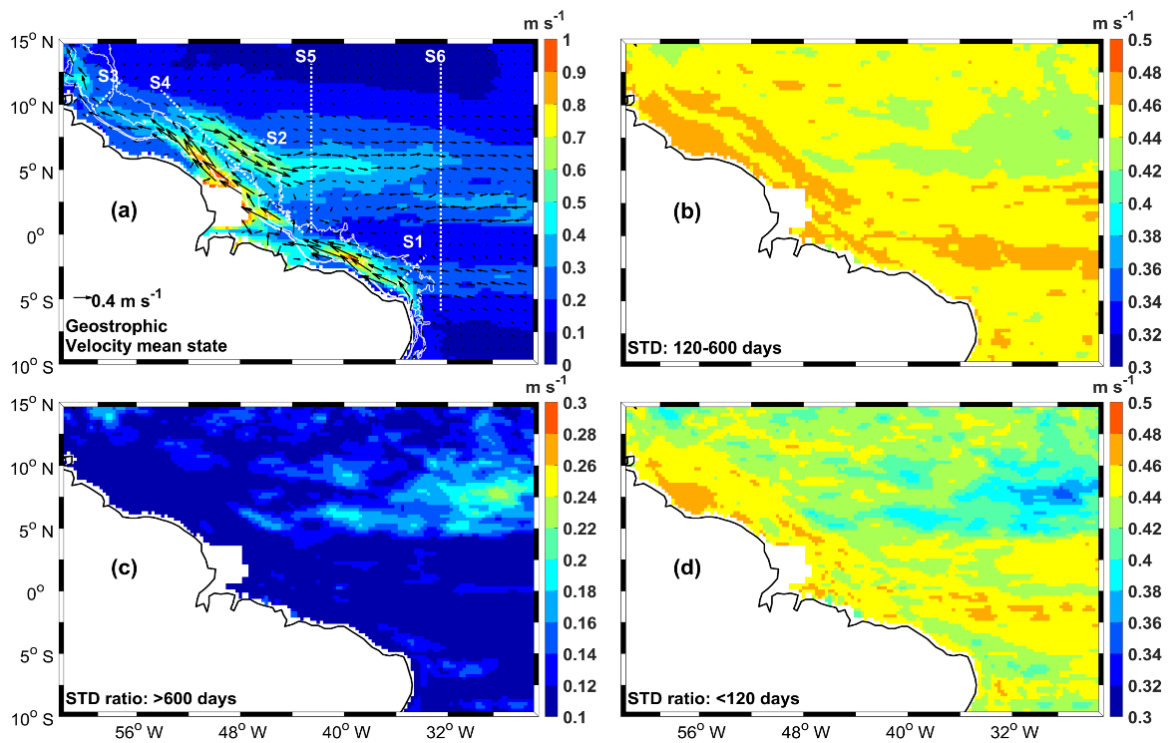
Figure 2. (a) Temporal mean of the geostrophic currents (amplitude in m s⁻¹ and vectors) in the study area between 1993 to 2017; **(b), (c)** and **(d)** ratios between the standard deviations of the currents for the signals between 120 and 600 days, longer~~more~~ than 600 days and shorter~~less~~ than 120days, respectively, and the standard deviation of the total currents. The white dashed lines S1, S2, S3, S4, S5, S6 in **(a)** represent the cross-sections of the currents, and the solid white lines are the 300 m, 1000 m, 3000 m and 4000 m isobaths. Note that, the colobar of **(c)** is different than the ones of (b) and (d).

312

313

314

315

316

317

318

319

320

321

322

323

324

325

Then we monthly averaged the daily geostrophic currents and extracted the cross-section geostrophic velocities along the six sections defined above (Fig. 1). In order to remove the intraseasonal variability, the monthly velocity estimates are further low-pass filtered using a 4-month cutoff frequency. The time-space diagrams (also called Hovmöller diagrams) along the six sections are plotted in Fig. 3. We can clearly observe large changes in both time and space with respect to the different current branches, illustrating the complexity of the surface circulation in the WTA. The seasonal and, in a lesser extent, the interannual current fluctuations mentioned above are clearly visible in the different sections. For each of them, the time-average current values are also computed as a function of the latitude (left-side plots in Fig. 3), highlighting the mean spatial extension of the current path~~vein~~s crossing the corresponding section. Note that in addition to the main currents mentioned in Fig. 1, between 2~~1.5~~° S-2° N, the sections 4 to 6 show an eastward surface current, ~~positioned~~located at the same location where the EUC flows, west of 44°W in the subsurface along the equator (Schott et al., 1998)~~might be located~~. Depending on the season the EUC core is known to be located between about 100-m depth and 50-m depth when it surfaces to reach the near-surface (Brandt et al., 2016). At 44° W, Bourlès et al. (1999b) have also noticed the presence of an ~~surface~~ eastward

surface flow above the EUC, which was identified to be different than the EUC. So, we chose to name it X hereinafter in order to further investigate this signal and its origin.

~~Table 1~~Table 2 summarizes the mean current width derived along the different sections (using left-side plots in Fig. 3). Note first that a positive current convention is chosen for the sections as follows: northward NBC along sections 1 to 3; eastward NBCR along section 4; eastward NECC along sections 5 and 6, and eastward X flows along sections 4 to 6. Hence, the signatures of the rNBC on the section 2, the nSEC (sections 4 to 6) and the cSEC (section 6) are considered as negative. From ~~Table 1~~Table 2, we observe that the NBC becomes narrower from the section 1 to the section 2. The retroflection zone (section S4, Fig. 3S4) extends from 3.7° N to 10.5° N, in agreement with Fonseca et al., (2004) who found the northernmost position of the NBCR around 11° N. North of the retroflection, the NBC along the Guyana coast is weaker, but broader relatively to the section 2 (NBC2 and NBC3 in Fig. 3). From section 6 to 4, the nSEC signature changes. It is wider at 32° W (nSEC6), then narrower at 42° W (nSEC5), and widens again closer to the shelf at 44° W (nSEC4) (respectively 550, 67 and 190 km in ~~Table 1~~Table 2). The NECC extension also varies from 32° W to 42° W, and is wider and located further north on the east, with a mean width extending from 860 km (NECC5) to 920 km (NECC6).

~~Table 1~~Table 2. Extension in latitude and km of the different currents branches crossing the different sections: NBC1, NBC2 and NBC3 are respectively the North Brazil Current captured on sections 1, 2 and 3; NECC5 and NECC6 are respectively the North Equatorial Countercurrent on the sections 5 and 6; nSEC4, nSEC5 and nSEC6 are respectively the northern branch of the South Equatorial Current (SEC) on the sections 4, 5 and 6; cSEC6 is the central branch of the SEC on the section 6; and X4, X5 and X6 are the equatorial eastward flow X on respectively on the sections 4, 5 and 6.

List of current path~~veins~~	Latitudinal coverage	Current width (km)
NBC1	1.3° S-4.6° S	~ 520
NBC2	3.6° N-5° N	~ 220
rNBC2	5° N-7.4° N	~ 380
NBC3	9.1° N-11.9° N	~ 440
NBCR4	3.7° N-10.5° N	~ 760
nSEC4	2° N-3.7° N	~ 190
X4	1.2° N-2° N	~ 120
NECC5	2.4° N-10.1° N	~ 860
nSEC5	1.7° N-2.3° N	~ 70
X5	0° N-1.7° N	~ 190
NECC6	4.1° N-12.4° N	~ 920
nSEC6	0° N-4.1° N	~ 550
X6	0° S-1.4° S	~ 110

cSEC6	1.4° S-5.9° S	~ 500

367

368

369

370

371

372

373

374

375

376

377

378

379

380

381

382

383

384

385

386

387
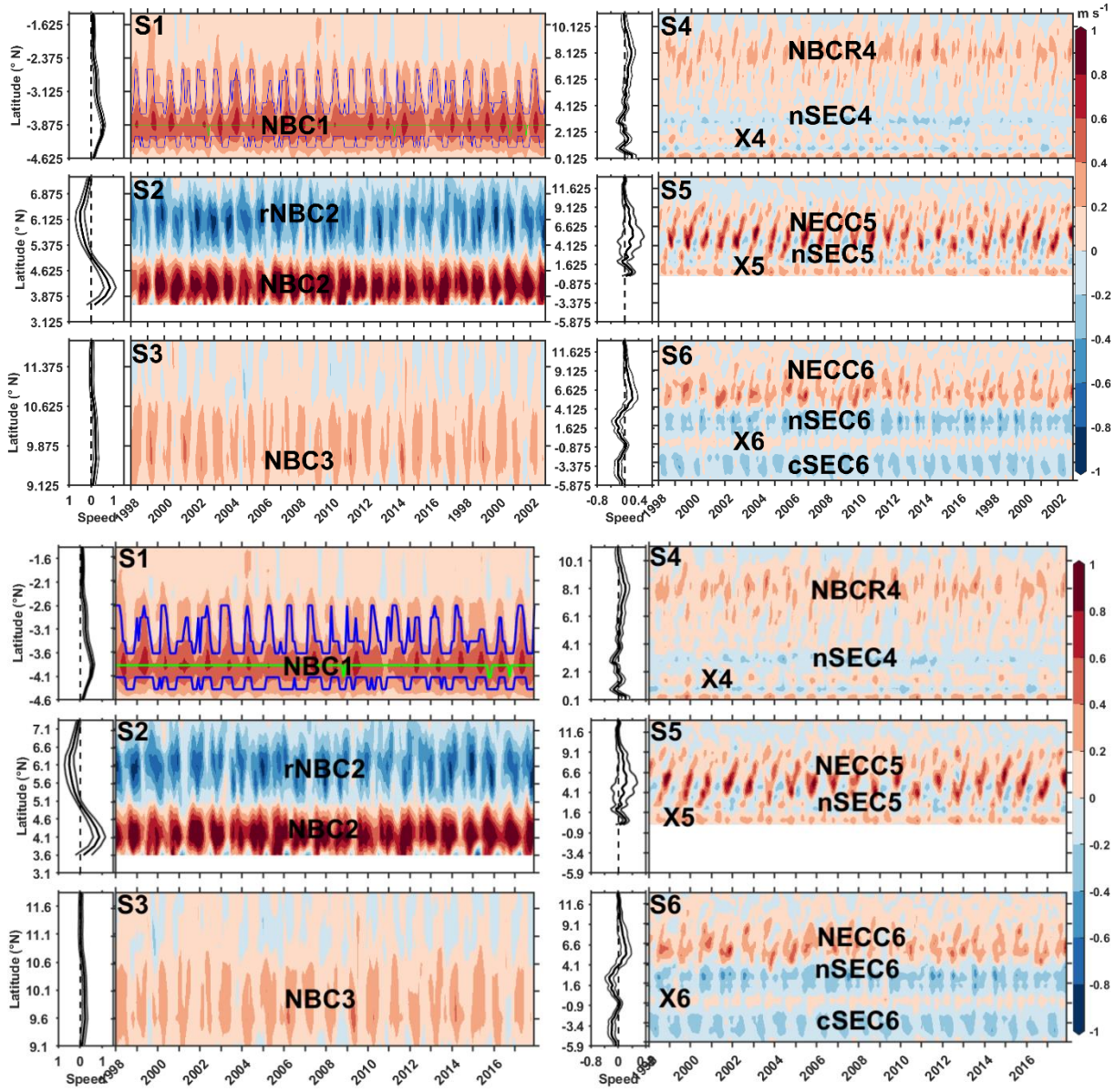
Figure 3. Hovmöller diagrams (1993 to 2017) of the cross-section current components (m s⁻¹) for S1, S2, S3 S4 S5 and S6. At the left of each diagram, the time series of time averages of the cross-section current (thick lines), framed by their corresponding standard deviations (thin lines) are plotted as a function of latitude. The red (blue) colors show the northward/eastward (southward/westward) directions of the cross-currents. Acronyms are listed in Table 1. : North Brazil current (NBC), its retroflected branch (rNBC) and the retroflection signature at the limit between the NBC and the rNBC (NBCR); North Equatorial Countercurrent (NECC); the equatorial surface eastward flow named X; northern and the central branches of the South Equatorial Current (nSEC and cSEC, respectively). The numbers next to the acronyms of the currents represents the number of the section. The green line in S1 indicates the time series of the maximum velocity of the cross-section current (NBC), and is framed by the time series of the maximum velocities divided by 2 (blue lines) over 1993-2017 period.

403
404
405
406
407
408
409
410
411
412
413
414

415 In order to further investigate the temporal variations of the current amplitude or strength, the
416 maximum speed~~velocity~~ values of each current paths~~vein identified in Table 1~~ have been
417 determined~~extracted~~ for each month. These maxima (corresponds to the current core and are
418 called Vmax hereafter: (see Fig. 3, green line on S1), and. t~~T~~heir location ~~of Vmax~~ corresponds
419 to the location of the current core. Then, to estimate the ~~corresponding~~ current relative
420 strength/intensity, we have considered the part of the sections of~~width is estimated, considering~~
421 ~~the part of the section where the~~ velociti~~es~~y ~~is~~ larger than Vmax/2 (see Fig. 3, blue lines on S1),
422 and we f. Finally computed, the strength~~relative~~/~~intensity~~ values~~is computed~~ by averaging the
423 ~~cross-section~~ velocity values of these parts over time~~he estimated current width. For each~~
424 ~~current vein crossing the six sections (Left column of Table 1), we compute the monthly time~~
425 ~~series of the resulting Vmax, current width and relative current intensity/strength.~~ The width of
426 the currents (Table 2) is determined by the mean of the current over the whole period of study
427 (1993-2017) at each grid point (see left boxes of the Hovmöller diagrams of Fig. 3). Then,
428 knowing the sign or direction of the current (eastward or westward), the corresponding time
429 series are used to define the width by finding the limits where the current is null. Note that the
430 current strength/intensity~~latter~~ has also been computed by averaging velocity values over the
431 entire width~~full transect~~ of the~~each~~ current paths~~vein~~ (e.g., not only where the velocity is larger
432 than Vmax/2), but the results did not correctly reflect the current variability observed in Fig. 3
433 and Fig. 4 (not shown).

434 For the NBCR and the NECC, the variability of the maximum speed (velocity) of the apparently
435 two flow/~~-~~branches and their corresponding locations is also analyzed, in order to compare with
436 the study of Fonseca et al. (2004). ~~It will also be used~~The goal is also to investigate the

variability of the current location with respect to the wind variability and to the tropical Atlantic climate modes. In this study, the presence of two ~~flows~~branches of the ~~e~~NBCR and the NECC two-core structure are identified when the ~~flow~~ velocity profile shows two local maxima separated by a local minimum respectively, in the NBCR region (considered between 4°-10° N) and the NECC region (considered between 3°-11° N) (Fig. ~~4~~S4-S6).
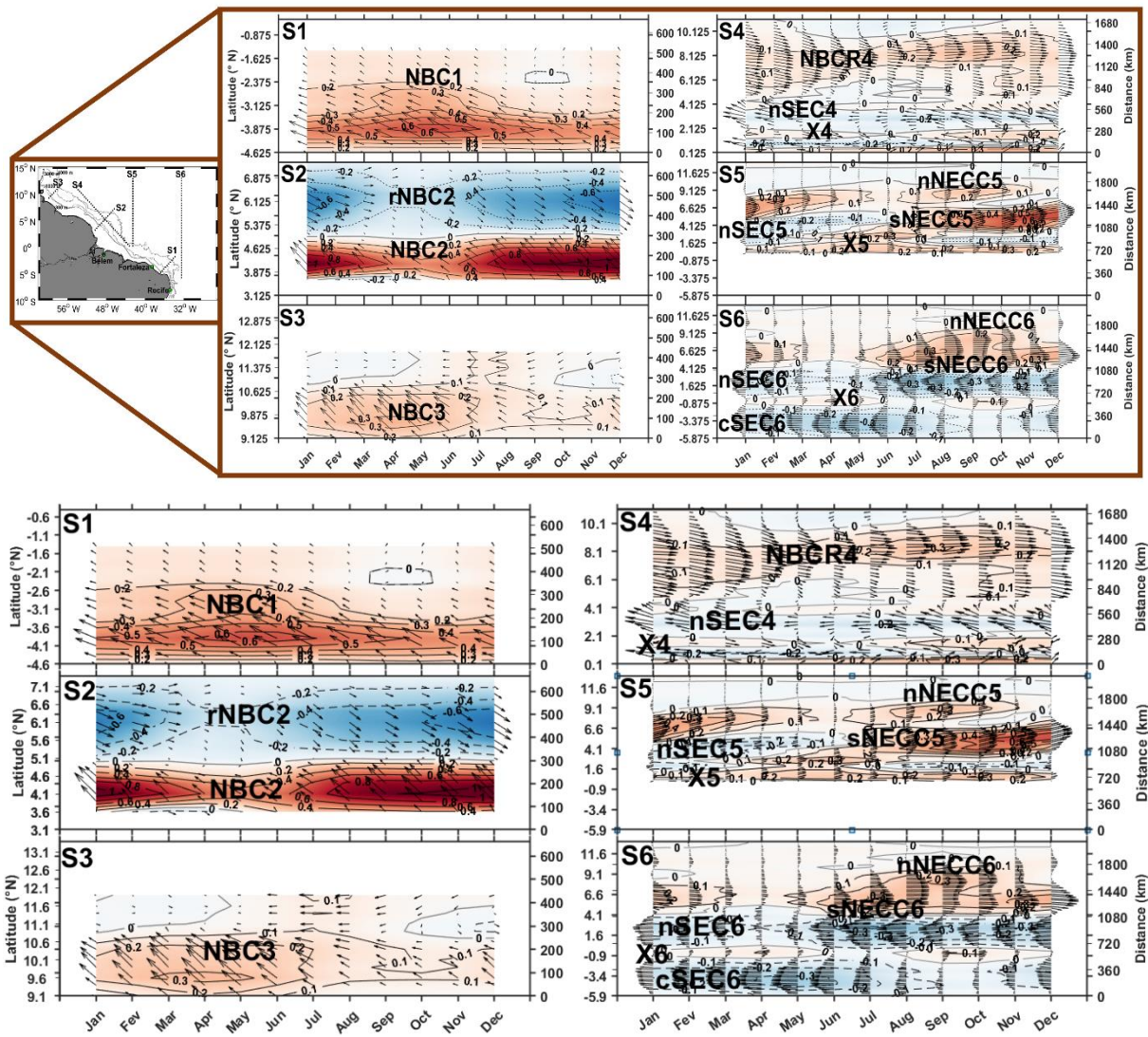
Figure 4. Average seasonal cycle obtained from Figure 3 ~~Hovmöller diagrams of the monthly climatology of the surface geostrophic~~ (vectors of the currents are superimposed on the contour of their amplitude in m s^{-1}) ~~over the 1993-2017 period. S1, S2, S3, S4, S5 and S6 are respectively for the sections 1 to 6 represented over the study~~

area (Left map). nNECC and sNECC are respectively, the northern and southern branches of the North equatorial Countercurrent (NECC); NBC, the North Brazil Current; NBCR, the NBC retroflection limit; rNBC, the retroflected branch of the NBC, nSEC and cSEC, the northern and the central branches of the South Equatorial Current, respectively; and X, the equatorial surface eastward flow. On the right sides of each subplotsdiagram, the distances from the southernmostlowest point (in km) are indicated.

4 Seasonal variability

Here we focus on the seasonal cycle of the different current branches observed in the study area. Therefore, a monthly climatology of the velocity estimates shown in Fig. 3 is calculated for each of the six sections (Fig. 4). For further analysis, the monthly climatology of Vmax, Vmax location, the current width and the relative current intensity has also been derived from the corresponding monthly time series for different current components ((Fig. 5). Ours analyses are presented inBelow, we analyze the following paragraphresults from the southeast to the northwest of the study area.
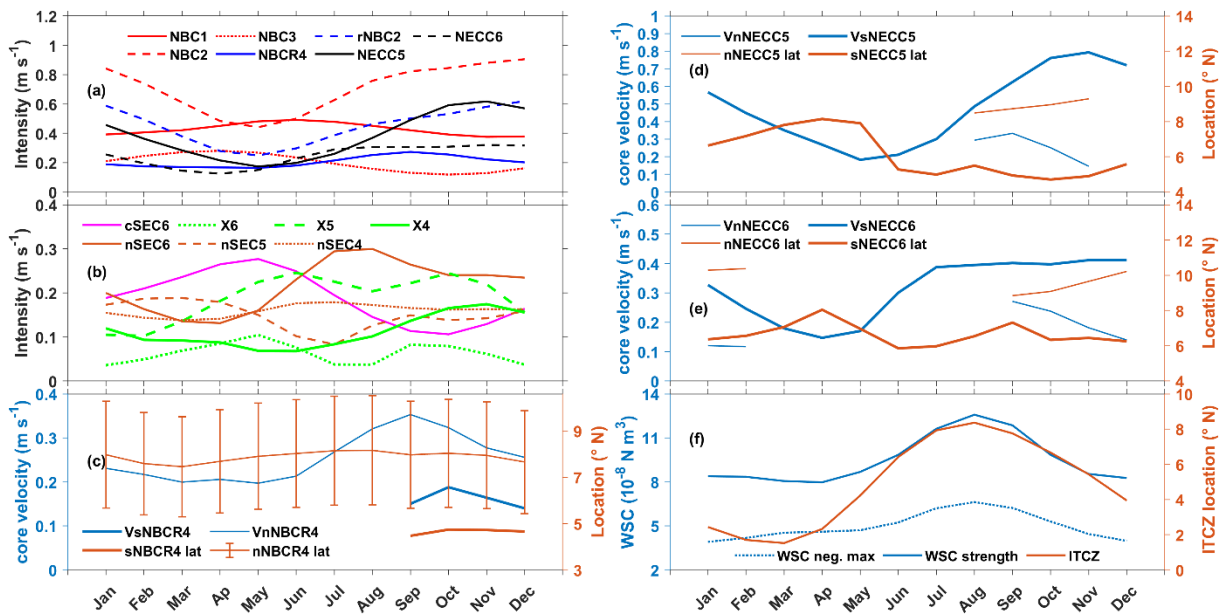
Figure 5. Monthly climatology of: the relative currents' ~~intensity~~ speed (m s^{-1}) **(a-b)**; the cores velocity/location in the ~~North Brazil Current Retroflection (~~NBCR~~)~~ regions **(c)**; the core~~s~~ velocity/location of the ~~North Equatorial Countercurrent (~~NECC~~)~~ branches along sections 5 and 6 **(d-e)**; and the absolute values of the maximum negative wind stress curl (WSC neg. max), the WSC strength and the ITCZ location **(f)**. ~~(a): NBC1, NBC2 and NBC3 represents the North Brazil Current (NBC) on the crossing sections 1, 2 and 3, respectively; rNBC2 represents the retroflected NBC branch (rNBC) crossing section 2; NBCR4, represents the NBCR flow crossing section 4; NECC5 and NECC6 represent the NECC crossing 5 and 6, respectively. (b) nSEC4, nSEC5 and nSEC6 represent the northern branch of the South Equatorial Current (SEC) crossing sections 4, 5 and 6, respectively; cSEC6 represents the central branch of the SEC crossing section 6; and X4, X5 and X6 represent the equatorial surface eastward flow X crossing sections 4, 5 and 6, respectively~~ Acronyms are listed in Table 1 and the numbers next to

the acronyms represents the number of the sections. On **(c)**, **(d)** and **(e)**, the ~~"V" initials/lat" at the end of each acronym represent~~ the core velocit~~y~~ies and location~~/~~s are respectively, in ~~(~~blue and ~~/~~orange color~~). The nNBCR/sNBCR and nNECC/sNECC represent the northern/southern core in the NBCR and the NECC regions, respectively.~~

4.1   The North Brazil Current and its retroflection

In Fig. 4, the NBC (Section 1) and the cSEC (Section 6) are observed both located at ~ 4° S and present similar seasonal cycles, with stronger flows during the first half of the year. The cSEC6 velocity maximum (0.3 m s^{-1}) / minimum (0.1 m s^{-1}) appears in May/October, respectively. The NBC1 velocity maximum (0.6 m s^{-1}) / minimum (0.4 m s^{-1}) appears in May-June/November-December (Fig. 5a). These annual cycles are also similar to the annual cycle of the NBUC transport observed by Rodrigues et al. (2007) at 10° S and which is related to the bifurcation location of the sSEC. This suggests that at its southernmost location, the seasonal variability of the NBC might be partly driven by the location of the sSEC bifurcation, which has been shown to be influenced by the annual cycle of the WSC over the area 5°–10° S, 25°–40° W (Rodrigues et al., 2007).

When comparing the NBC along sections S1, S2, S3 and S4 (Fig. 4S1-S4 and Fig. 5), it clearly depicts two different seasonal cycles along its northward path. The NBC2, NBCR4 and the rNBC2 flows show approximately the same seasonal cycles, in opposite phase with NBC1 and NBC3 ones, approximatively in phase. NBC2 is narrower but relatively stronger than NBC1. It decreases from January to May (by ~ 0.4 m s^{-1}), and then increases again to reach a maximum in November-December (1 m s^{-1}). Compared to NBC2, the rNBC2 is broader (width of ~ 350 km against 200 km) but less intense (maximum of 0.6 m s^{-1} in November-December). Apparently, the NBC2 width and strength seem to be linked to the nSEC intensity in the eastern

basin (see nSEC6 and nSEC4 in Fig. 5b). When the nSEC is weaker, the NBC2 is also weaker and narrower. Then, the NBC2 starts growing one month later when the nSEC intensity is increasing. This shows the importance of the nSEC contribution to the NBC to the north of the equator. The delay between the nSEC and NBC2 growth can be due to the mesoscale activities more intense in the western basin (Aguedjou et al., 2019). The fact that the NBC1 and the NBC3 are in phase when the nSEC contribution to the NBC2 is lower might also indicate that the NBC is more stable when the intrusion of water from the nSEC is weak. And then, most of the NBC in the upper layer tends to follow its northward route. Contrariwise, when the current is unstable because of the barotropic and baroclinic instabilities generated by the nSEC, most of the NBC flow tends to retroflects eastward. This can justify the phase of the NBC2, NBC4 and rNBC2. In Fig. 4, from September to January, we observe two retroflections of the NBC: the main one around 8°N and a secondary one more to the south, between 4-6° N (Fig. 4S4 and 5c). The flow of this secondary retroflection (called sNBCR) reaches its maximum intensity in October while the main retroflection flow (called nNBCR) reaches its maximum one month earlier. Then, it migrates northward to join the nNBCR4; and both are completely merged at the beginning of the following year (Fig. 4S4). Both branches merge at the beginning of the year and the NBCR then weakens to reach its minimum intensity in May. Note that the seasonal cycles of the NBC2 and the NBCR have are similar to the one of the NBC transport obtained by Johns et al. (1998) and Garzoli et al. (2004) using acoustic Doppler current profilers (ADCP)/Inverted Echos sounders/Pressure gauge data. Johns et al. (1998) related the seasonal cycle of the NBC observed in this area to the remote wind stress curl forcing across the tropical Atlantic. Here, we also see that the seasonal cycles of the NBC branches north of the equator (except the NBC continuity along the Guyana coast) seems to follow the remote wind stress curl strength with a delay of by one to four months (Fig. 5a-f). Because of the instabilities of the region, the delay should be impacted by the mesoscale activities and/or wave propagations in the region (Fonseca et al., 2004). The northernmost location of the nNBCR maximum intensity occurs in August, when the maximum WSC strength is reached (Fig. 5c, f). The root mean square (rms) of the monthly mean values of its location (Fig. 5c) is nearly constant (~2.3°), and is consistent with the evidence that there may not be a preferred season for NBC ring formation (Garzoli et al., 2003; Goni and Johns, 2003). Indeed, Garzoli et al. (2003) have shown using inverted echo sounder observations that there was a link between the rapid northward/southward extension of the NBC retroflection and the shedding of the rings in this region.

564   Faurther north, the NBC component flowing along the Guyana coast (NBC3) is twice wider (~

565   440 km) and less intense than the NBC2 (Fig. 4S2-S3). It reaches a minimum in October (~ 0.1

566   m s^{-1}), and a maximum during March-May (0.3 m s^{-1}) when the NBCR4 is minimum (Fig. 4S3-

567   S4 and 5). As already mentioned, its seasonal cycle is similar to the NBC1 and cSEC, and might

568   also be influenced by the sSEC bifurcation location.

569   4.2   The North Equatorial CounterCurrent

570   The NECC (both NECC5 and NECC6) seasonal cycle is similar to the ones of the NBC2,

571   NBCR4 and rNBC2 (Fig. 4S2, S4, S5-S6). It weakens along its pathway and its intensity is

572   maximum in November-December (~ 0.6 m s^{-1} at 42° W and ~ 0.3 m s^{-1} at 32° W), and

573   minimum in April-May (Fig. 5a). During the second part of the year, we observe the two-core

574   structure previously investigated by Urbano et al. (2006; 2008). The two cores/branches are

575   seen first at 42° W in August, then at 32° W in September (Fig. 4 and 5d-e). The northern

576   branch (nNECC) is narrower (located between 7°-9° N) and stronger (0.3 m s^{-1}) in August-

577   September at 42° W (Fig. 4S5 and 5d). It is even separated from the southern branch from

578   October to December. At 32° W, the NECC appears with one single core from September

579   (northern core velocity of ~ 0.2 m s^{-1}) to November. The northern core is gradually decreasing

580   in intensity and shifting northward until forming a separated second branch, which is located

581   between 9-11° N from December to February, and then becomes very weak in March-April

582   (Fig. 4S5 and 5e). From June to July, the NECC signature (sNECC branch) is located between

583   3-4° N at 42° W, and is connected from the south to the eastward flow associated with X5 in

584   Fig. 4S5. Urbano et al. (2008) showed with ADCP data at 38° W that the eastward ~~flow south~~

585   ~~of the~~ NECC cycle may start in this region when the EUC is shallower and further north, and

586   seems to be connected also to a shallower~~corresponds to the mixing of~~ NEUC ~~and EUC waters~~

587   during this period of the year. The presence of the equatorial surface eastward flow X5 suggests

588   that this latter may be the one that favors the surfacing and the connection of both currents

589   during June-July. From June to November, the sNECC branch increases simultaneously with

590   the rNBCR2. However, it reaches its maximum one month earlier (November) and start

591   decreasing when the rNBC is still increasing. This confirms that the NECC is not only fed by

592   the rNBC at the surface as suggested by Verdy and Jochum, 2005. The sNECC witnesses the

593   same variability at both 32° W and 42° W, but reaches its minimum early in March-April at 32°

594   W when the climatological NECC is described in the literature as a reversing flow or is missing

595   at its usual location (Garzoli and Katz, 1983; Garzoli, 1992). At this location (32° W), the

596   sNECC starts increasing from April-May, between 4°-6° N far from the eastward flow X, and

597 grows until November. Burmeister et al. (2019) showed that, in the central Atlantic, when the

598 ITCZ migrates northward (April to August) (Fig. 5f), the nSEC recirculate~~d~~s eastward to reach

599 the NEUC which then increases. The presence of the sNECC flow in April-May may suggest

600 that the NECC flow might be initiated by an eastward~~the~~ recirculation of the nSEC which

601 ~~should~~ flows on top of the~~mix with the upper~~ NEUC ~~water~~ during this period. It reaches its first

602 maximum in July-August together with the nSEC, and a second maximum in November (Fig.

603 5a, b, e). At 32° W and 42° W the sNECC shows two northward migrations. The first migration

604 occurs from June-July (June) to August (September) at 42° W (32° W), and the second occurs

605 from October to April (Fig. 5d-e). Fonseca et al. (2004) also found such behaviors but with

606 some differences: two northernmost NECC locations in February and August, and two

607 southernmost NECC locations in June and December. But they lacked data between March and

608 May, and we do not use the same methods to compute the core position.

4.3   The central and northern branches of the South Equatorial Current

610 Obviously,~~Although~~ the cSEC and nSEC which are two branches of the westward SEC ~~flow,~~

611 ~~they~~ do not have the same seasonal cycle (Fig. 4S4, S5, S6). This is due to the fact that, in the

612 northern hemisphere, the nSEC is affected by the southerlies which cross the equator, inducing

613 a migration of the ITCZ location. However, t~~T~~he cycles of the nSEC4, nSEC5 and nSEC6 have

614 maxima at different periods of time. At 32° W, the nSEC (nSEC6) increases from April to reach

615 a maximum of ~ 0.3 m s^{-1} in August, following the migration of the ITCZ (Fig. 5b, f). During

616 this time, at 42° W, the nSEC (nSEC5) migrates northward, and its intensity decreases until

617 July, when it almost disappears. The eastward flow X then appears (Fig. 4S5). The nSEC5 is

618 observed again after July, increases and reach a maximum of ~ 0.2 m s^{-1} in March (Fig. 4S5,

619 S6 and Fig. 5b). Over the continental shelf, most of the nSEC joins the NBC (section 4, around

620 2-4° N and 46° W) and a part ~~of the flow~~ deviates southeastward to join the rNBC and form the

621 eastward flow X4 (captured along section 4, Fig.4S4). The nSEC component that joins the NBC

622 reaches its maximum of ~ 0.2 m s^{-1} between June and August (also following the ITCZ

623 northward migration, Fig. 5b, f). However, the nSEC seasonal variations are relatively small (~

624 0.15 m s^{-1}) (Fig. 4S4). It is particularly true for nSEC4 but the angle of the section relative to

625 the flow probably leads to a significant reduction of the current amplitude captured.

4.4   The eastward current X

627 Figure 4S4-S6 show~~s~~ the presence of an eastward current near the equator. Such feature was

628 already observed and mentioned by Hisard and Hénin (1987) and Bourles et al. (1999b) using

629 hydrographic and ADCP data. In Fig. 4S4, eastward flows are captured between 1-2° N (X4)

630 and along the equator. As mentioned in Sect. 4.3, they may be composed of the part of the nSEC

631 that does not join the NBC and the rNBC (which is kn~w~own to feed the EUC in the thermocline

632 layer). The weaker intensity of X4, compared to X5 (i.e. X at 42) is explained by the angle

633 between S4 and the current direction. But the weaker intensity of X6 (i.e. X at 32° W) is due to

634 the weakening of the corresponding eastward flow between both longitudes. X4 and X5 are

635 observed almost throughout the year (Fig. 4S4-S6) and their amplitude follows a semi-annual

636 cycle (Fig. 5b) similar to the EUC in the eastern Atlantic (Hormann et al. 2007). However, the

637 periods of the maxima are slightly different from ~~one~~ location to ~~the an~~other. X4 displays a

638 semi-annual cycle, with a weak maximum in March-April (~ 0.1 m s^{-1}) and another maximum

639 in November (~ 0.2 m s^{-1}). X5 amplitude is larger because of the merging of X4 with the

640 eastward flow ~~seen~~ observed along the equator (Fig. 4S5). Its maxima occur in June and

641 October with similar intensity (more than 0.2 m s^{-1}) (Fig. 5b). X6 (at 32° W) is weaker, but

642 reaches its maxima in May and September-October (less than 0.1 m s^{-1}). Since this eastward X

643 flow is almost not documented in the literature, we will come back to it in Sect. 6.

644 **5   Interannual variability**

645 Beyond the dominant seasonal variability of the circulation at regional scale, we also observe a

646 year-to-year variability of the surface velocities in the study area (Fig. 2 and Fig. 3). The latter

647 is analyzed here, using the time series of the characteristics of the different current branches

648 (see end of Sect. 3) captured along the 6 sections (Fig. 6). We will also analyze this variability

649 in the light of the tropical Atlantic climate modes.

650

651
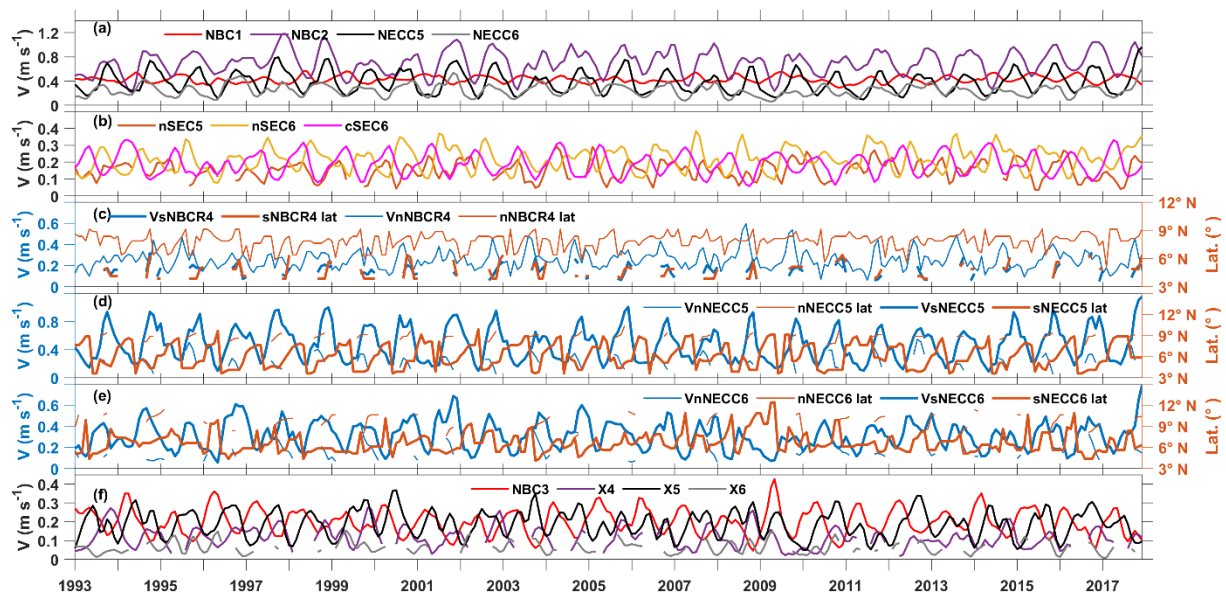
Figure 6. Time series of the 4-month low-pass filtered characteristics of the geostrophic currents **(a-f)** captured along sections 1 to 6. Acronyms are listed in Table 1 and the numbers next to the acronyms represents the number of the sections **(a)**: intensity of NBC1 ~~crossing the sections 1 (NBC1)~~ and 2 ~~(NBC2)~~, and of the ~~NECC crossing the sections 5 (~~NECC5~~)~~ and 6 ~~(~~NECC6~~)~~. **(b)**: intensity of the ~~cSEC crossing the section 6 (~~cSEC6~~)~~ and of the ~~nSEC crossing the sections 5 (~~nSEC56 and 6 ~~(~~nSEC6~~)~~. **(c)**, **(d)** and **(e)** core velocities and the locations of ~~the northern and southern cores of~~ respectively the nNBCR4 ~~and the~~ sNBCR4 flows ~~crossing the section 4 (NBCR4)~~, ~~and of the NECC cores on sections 5 (the n~~NECC5, ~~the) and 6 (s~~NECC5, the nNECC6 and the sNECC66~~)~~. **(f)** Intensity of the NBC ~~crossing the section 3 towards the Guyana coast (~~NBC3~~)~~, ~~and the equatorial surface eastward flow crossing the sections 4 (~~X4~~)~~, 5 ~~(~~X5~~)~~ and 6 ~~(~~X6~~)~~. ~~The "V" initials at the beginning, and "lat" at the end of each acronym of the legends in (c), (d) and (e) represent the core velocity and location, respectively (blue and orange colors, respectively). The thin (tick) lines represent the northern (southern) branches of these currents/flows.~~

In Fig. 6a-b we observe that over the whole study period the intensities of the cSEC6 (cSEC along section 6) and of the NBC1 (NBC along section 1) and NBC2 (NBC along section 2) vary between 0.05-0.35 m s^{-1}, 0.3-0.6 m s^{-1} and 0.2-1.2 m s^{-1}, respectively. with corresponding mean values of 0.2 m s^{-1} $\pm$ 0.06, 0.4 m s^{-1} $\pm$ 0.06 and 0.7 m s^{-1} $\pm$ 0.2. To the north, when crossing section 3, the NBC weakens and ranges between 0.05-0.43 m s^{-1} with a mean intensity of 0.2 m s^{-1} $\pm$ 0.07. In the equatorial region ($\pm 5°$ of latitude), along sections 5/6, the nSEC intensity varies between 0.05-0.3 m s^{-1}/0.1-0.4 m s^{-1}, with a mean value of 0.15 m s^{-1} $\pm$ 0.05/0.2 m s^{-1} $\pm$ 0.07 (Fig. 6b). The eastward flow X intensity vary between 0.15-0.3 m s^{-1}, 0.05-0.4 m s^{-1} and 0-0.15 m s^{-1} when crossing sections 4, 5 and 6, respectively, with corresponding mean values of 0.12 m s^{-1} $\pm$ 0.05, 0.2 m s^{-1} $\pm$ 0.07, and 0.06 m s^{-1} $\pm$ 0.03.

683 ~~As mentioned in Sect. 3, the interannual variability is more important in the eastern part of the~~
684 ~~basin, and especially in the NECC region.~~ The two-core structure of the NECC and the NBCR
685 regions show the highest year-to-year variations in both velocity and location (Fig. 6c-e). The
686 NECC/NBCR time series were found significantly correlated (>0.98) in terms of both intensity
687 and core velocity (sNECC and nNBCR; ~~f~~Figure not shown). At 42° W, the sNECC/nNECC)
688 velocity core~~s~~ var~~ies~~ between 0.1-1.2 m s^{-1}/0.05-0.55 m s^{-1}, with ~~a~~ mean value~~s~~ of 0.5 m s^{-1} ±
689 0.25 /0.25 m s^{-1} ± 0.1. They~~It~~ are~~is~~ located between 3.6°-9.9° N/7.6°-10.4° N, with ~~a~~ mean
690 location~~s~~ at 6.1° N ± 1.7°/8.9° N ± 0.8° (Fig. 6d). At 32° W, the cores~~it~~ var~~ies~~ between 0.05-
691 0.8 m s^{-1}/0.05-0.5 m s^{-1}, with ~~a~~ mean velocit~~i~~es~~y~~ of 0.3 m s^{-1} ± 0.13/0.2 m s^{-1} ± 0.09. They are~~It~~
692 ~~is the~~n located between 4.1°-12.4° N/7.4°-11.6° N, with ~~a~~ mean location~~s~~ of 6.6° N ± 1.4°/9.7°
693 N ± 1.1° (Fig. 7e). The sNBCR /nNBCR maximum speeds~~velocity~~ crossing the section 4 varies
694 between 0.05-0.3 m s^{-1}/0.05-0.6 m s^{-1}, with ~~a~~ mean value~~s~~ of ~ 0.15 m s^{-1} ± 0.06/0.25 m s^{-1} ±
695 0.08. And, they are~~It is~~ located between 3.9°-6.4° N / 5.1°-9.1° N, with ~~a~~ mean location~~s~~ of 4.7°
696 N ± 0.8°/7.9° N ± 0.8°. Northeast of the equator, for all these current branches, we observe
697 important year-to-year variations, both in terms of current core location and of velocity
698 amplitude.

699 For further analysis, the anomalies of the current's characteristics (intensity and core
700 value/location) relative to their monthly climatology have been computed (Fig. 7). First, we do
701 not see obvious relationship between the different resulting monthly anomaly time series over
702 the whole period investigated. No relationship was found between ~~the evolution of~~ the intensity
703 of the NECC branches ~~intensity/core value and their location,~~ or of the NBCR flows ~~maximum~~
704 ~~velocity~~ and their location. However, for some particular years, both the NECC intensity/core
705 velocity and location show significant anomalies at 32° W. For example, the monthly anomalies
706 of the sNECC6 location were shifted far to the north / south in 2009 and 2010 / 1996 and 2001.
707 Simultaneously, the monthly anomalies of the sNECC6 intensity/core value were unusually
708 weak / strong (Fig. 7f-g).

709 To investigate the relationship between the AMM, the AZM, and the year-to-year variability of
710 the characteristics of the different current~~s~~ at different locations~~branches between~~ over 1993-
711 ~~and~~ 2007 period, we computed the three-month ~~running mean~~average anomalies centered each
712 month ~~of both~~ the ~~monthly anomaly~~ time series of the current anomalies and of the climate
713 mode indexes (so-called 3-month anomaly time series). So, the AMM and AZM peak events
714 (respectively, March-April-May and June-July-August)~~The latter~~ have been correlated with
715 ~~each other~~the 3-month anomaly time series of the currents in order to learn more about ~~the~~

716 ~~spatio temporal characteristics of~~ their possible relationship at the interannual

717 timescale~~variability~~ in the study area (~~f~~Figures not shown). Only the correlations greater than

718 ±0.5 and which have been found significant with 95 % of confidence level, performing the

719 Student's test are discussed below (listed in ~~Table 2~~Table 3).

720

721

722

723

724

725

726

727

728

729

730

731

732

733

734

735

736
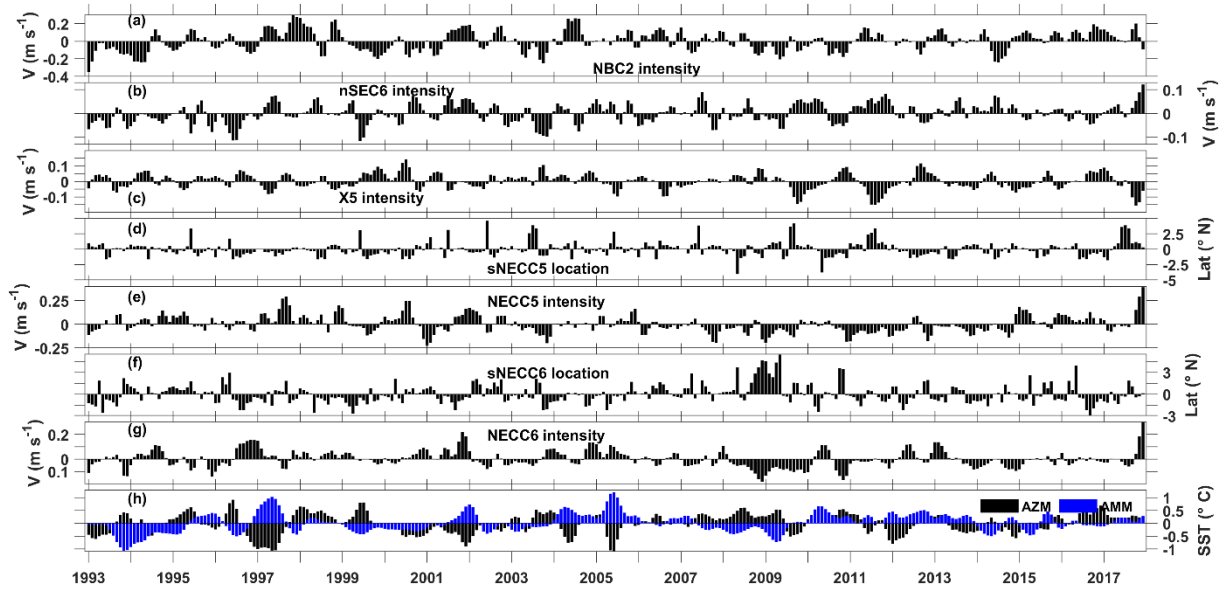
Figure 7. Time series of monthly anomalies relative to the monthly climatology for: **(a)**, the NBC2 intensity ~~on the section 2~~; **(b)**, the nSEC6 intensity ~~on the section 6~~; **(c)**, the equatorial surface eastward flow X5 intensity ~~on the section 5~~; **(d)**, the sNECC5 core location ~~on the section 5~~; **(e)**, the NECC5 intensity ~~on the section 5~~; **(f)**, the sNECC6 core ~~position on the section 6~~location; and **(g),** the NECC6 intensity ~~on the section 6~~; **(h),** Normalized indexes of the ~~tropical Atlantic meridional mode~~ (AMM ~~(:~~blue color) and ~~zonal mode~~ (AZM ~~(:~~black color).

Table 2Table 3. Correlations values between the characteristics of the current branches and the Atlantic meridional and zonal mode indexes (AMM and AZM, respectively). Where the correlations are found lower than 0.5, we indicate "insignificant" over the whole time period ("none"). The current branches analyzsed are the NBC (North Brazil Current), the sNECC (southern branch of the NECC), the nSEC (the northern branch of the South Equatorial Current) and the equatorial eastward flow called X.

Current branches' characteristics		Atlantic meridional mode (AMM) during March-April-May	Atlantic Zonal mode (AZM) during June-July-August
NBC1 intensity (section 1)	Correlation	Higher than -0.51	Insignificant
	Period	June-July	None
NBC2 intensity (section 1)	Correlation	0.58	Insignificant
	Period	March-April-May	None
sNECC5 intensity (section 5)	Correlation	Insignificant	-0.51
	Period	None	September
sNECC6 intensity (section 6)	Correlation	Higher than 0.50	Insignificant
	Period	March-April-May	None
sNECC6 core location (section 6)	Correlation	Higher than 0.51	Insignificant
	Period	March-April-May	None
nNECC6 core location (section 6)	Correlation	-0.62	Insignificant
	Period	March	None
nSEC5 intensity (section 5)	Correlation	Insignificant	-0.52
	Period	None	November
nSEC6 intensity (section 6)	Correlation	Higher than 0.52	Insignificant
	Period	March-April-May	None
Equatorial eastward flow X (Sections 4 and 5)	Correlation	Higher than -0.55	Insignificant
	Period	May-June	None
Equatorial eastward flow X (Section 6)	Correlation	Higher than 0.62	Higher than -0.52
	Period	March-April-May	June-July

769 The AMM index is found anticorrelated with the NBC intensity along the section 1 during

770 March-April-May, the nNECC core location along the section 6 and the equatorial eastward

771 flow (X) intensity west of 42° W, with respective coefficient of correlation (cc) higher than -

772 0.51 during June-July, about -0.62 in March, and higher than -0.55 in May-June. These anti-

773 correlations show the probability of the positive (negative) AMM phases to lead the negative

774 (positive) anomalies of the nNECC core location at 32° W with 0-month delay, the negative

775 (positive) NBC intensity between 3°-5° S and the X flow intensity anomalies (west of 42° W)

776 with 1- to 2-month and 0- to 1-month delay, respectively. However, the AMM index during

777 March-April-May is found correlated with the NBC intensity north of the equator before the

778 retroflection (cc ~0.58) and, the sNECC intensity/core location and the nSEC intensity at 32°

779 W (cc higher than 0.50/0.51 and cc higher than 0.52, respectively) during the same period of

780 time. This suggests that the positive (negative) AMM phases probably drives the positive

781 (negative) anomalies of the corresponding currents with no time lag.

782 During June-July-August, the AZM index is found anticorrelated with the sNECC/nSEC

783 intensity at 42° W (cc=-0.51/-0.52) only in September/November. This~~It~~ suggests that the

784 positive (negative) AZM phases probably lead the negative (positive) anomalies of the

785 sNECC/nSEC intensity with 1- and 3-month delay, respectively.

786 The eastward flow X intensity at 32° W is found simultaneously correlated with AZM and

787 AMM in June-July and March-April-May, with cc higher than 0.62 and -0.52, respectively.

788 This suggests that the positive (negative) anomalies of X at 32° W might be associated with

789 both positive (negative) AZM and negative (positive) AMM phases with no delay.

790 Referring to Cabos et al. (2019), the relationships found between the currents and the AMM

791 show the influence of the strengthening ~~/ weakening~~ of the southeast trade winds ~~in the southern~~

792 ~~hemisphere~~ on the southward ~~/ northward~~ migration of the nNECC core at 32° W, whereas the

793 NBC intensity between 3°-5° S and the equatorial eastward flow X intensity west of 42° W

794 decrease, and ~~vice versa / increase~~. Conversely, the strengthening ~~/ weakening~~ of the southeast

795 trade winds ~~in the southern hemisphere~~ should~~may~~ influence the northward ~~/ southward~~

796 migration of the sNECC core at 32° W, whereas the NBC2, sNECC6 and nSEC6 intensities

797 increase, and ~~vice versa / decrease~~. Referring to the same authors, the relationship with the

798 AZM ~~should~~ indicates the probable influence of the positive ~~/ negative~~ westerlies anomalies in

799 the western part of the basin on the negative ~~/ positive~~ anomalies of the sNECC and nSEC

800 intensities at 42° W, and vice versa. Concerning the eastward flow X at 32° W the relationship

801 with both the AZM and the AMM modes ~~should~~ indicate its strengthening ~~/ weakening~~ during

802 the concurrent events of positive ~~/ negative~~ westerlies anomalies in the western part of the basin

803 and the negative ~~/ positive~~ southerlies winds anomalies, and vice versa ~~in the southern~~

804 ~~hemisphere~~.

6 Discussion

806 Finally, we have computed the seasonal maps of the geostrophic currents in the whole WTA

807 (Fig. 8) in order to have a regional view of the seasonal variations of the circulation. Fig. 8

808 confirms the results obtained from the analysis of the cross-section velocities in Sect. 4 (in terms

809 of seasonal cycles and spatial structure) but also highlights interesting new features.

810 A large cyclonic circulation is observed between 35°-45° W and 0°-5° N during boreal spring

811 (blue ellipse). The latter is formed by the westward nSEC which is suddenly deviated to the

812 northeast by the presence of an eastward flow at ~32° W. Then, near 44° W and 5° N, the nSEC

813 meets the rNBC which reaches it southernmost position during this season, and deviates to the

814 southeast. When reaching the equatorial region between 0°-2° N, where the equatorial eastward

815 flow is found (Fig. 4), the resulting flow becomes stronger, and is deviated to the east, close

816 this cyclonic feature. This finding might answer the question of Schott et al. (1998) about the

817 destination of the rNBC during spring, when the rNBC does not feed the NECC anymore. From

818 German cruises SADCP measurements (downloaded from the data center PANGEA

819 https://doi.pangaea.de/10.1594/PANGAEA.937809 and described in Tuchen et al, 2022), the

820 zonal and meridional components of currents over the equatorial region have been analyzed

821 (40°W, 35°W and 32°W: figures in supplementary material). They confirm the existence of the

822 equatorial surface eastward flow, with a shifting tendency at 35°W to the north. During the

823 boreal winter, another cyclonic circulation is observed between 44°-50° W and 5°-10° N (blue

824 ellipse in Fig. 8): part of the NECC recirculates north-westward to join the rNBC. During both

825 boreal winter and spring, ~~a~~ south-westward recirculations of the NECC appear to strengthen the

826 nSEC located west of 32° W. This~~It~~ is consistent with the increase of the nSEC intensity

827 observed along section 4, compared to the nSEC intensity captured along section 6, between

828 February and May (Fig. 5b).

829 During the second half of the year, Fig. 8 shows a wider NECC which extends north of 10°N.

830 During boreal fall, the NECC flow is formed by a nNECC branch separated from the initial

831 sNECC branch during between 38°-48° W, that meet east of 38° W. This is consistent with Fig.

832 4 S5-S6. During boreal summer, the nNECC branch seems to be supplied by the northern part

833 of the NBC retroflection. This connection seems to fade during boreal fall.

834 In the equatorial region (2° S-2° N), Fig. 8 also shows an equatorial eastward flow X with lower

835 amplitude which appears to be extended east of 32° W and stronger during boreal spring and

836 fall. This feature can be related to the near-surface eastward flow mentioned by Hisard and

837 Hénin (1987) and Bourlès et al. (1999b) on top of the EUC in the WTA. Hisard and Hénin

838 (1987) explained the poor description of this current in the literature by the difficulty of ADCP~~s~~

839 measurements to fully capture the upper layer currents in this area. They showed that this near-

840 surface current, independent from the EUC, can reach amplitudes larger than 0.5 m s⁻¹ between

841 23° W and 28° W. In this study, ~~order to understand this difference in current amplitude,~~

842 ~~compared to ours (~ 0.1 m s⁻¹), we computed~~ the seasonal maps of the near-surface Ekman

843 currents (figure not shown~~Fig. 9~~). ~~We observe~~ showed westward currents with higher

844 amplitudes in this equatorial band (larger than 0.2 m s⁻¹) compared to X, mostly east of 32°W.

845 Then, we conclude that the near-surface velocities found here~~in this study~~ in the equatorial

846 region should be~~are~~ underestimated, particularly in the eastern basin.~~, compared to~~ This is

847 consistent with the strengths of the X current found ~~absolute surface velocities~~ in ~~(~~Fig. 5b~~)~~.

848 For the first time, the seasonal cycle of the equatorial eastward flow has been analyzed in Sect.

849 4.4 of this study (Fig. 4S4, S5, S6 and Fig. 5b). It is similar to~~with~~ the seasonal cycle of the

850 EUC (semi-annual cycle with two maximum), which might be due to the fact that most part of

851 the flow is fed by the rNBC.

852

853

854

855

856

857

858

859

860
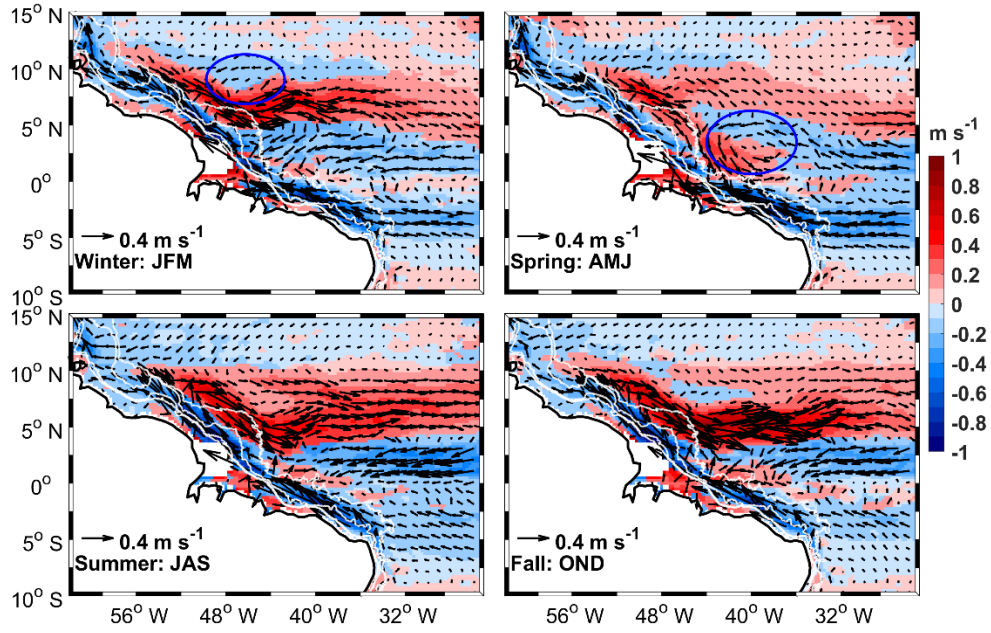
861 **Figure 8.** Seasonal maps of the geostrophic currents in the western tropical Atlantic over the 1993-2017 period

862 for boreal winter (top left panel: JFM for January-February-March), boreal spring (top right panel: AMJ for April-

863 May-June), boreal summer (bottom left panel: JAS for July-August-September:) and boreal fall (bottom right

864 panel: OND for October-November-December:). The velocity vectors are superimposed on the ~~speed~~velocity

865 ~~amplitudes~~ multiplied by the sign of their ~~zonal~~horizontal components (m s^{-1}). The two cyclonic circulations

866 observed during boreal winter and spring are indicated by blue ellipses. The white lines near to the continent are

867 from west to east, the 300 m, 1000 m, 3000 m and 4000 m isobaths.

868

869

870

871
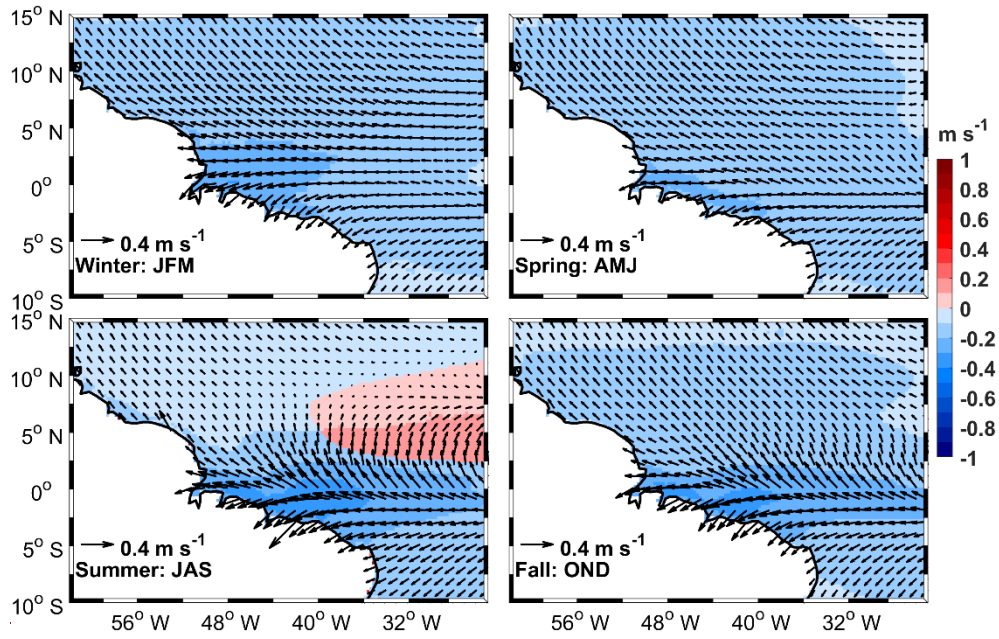
Figure 9. Seasonal maps of the Ekman currents in the western tropical Atlantic over the 1993-2017 period for boreal winter (top left panel: JFM for January-February-March:), boreal spring (top right panel: AMJ for April-May-June), boreal summer (bottom left panel: JAS for July-August-September) and boreal fall (bottom right panel: OND for October-November-December). The velocity vectors are superimposed on the velocity amplitudes multiplied by the sign of their horizontal components (m s^{-1}).

891   From the analyses offinally, the current analysis madecarried out above, allows us to derivewe
892   propose a new scheme of the seasonal variations of the western boundary tropical Atlantic
893   circulation (Fig. 910). The new current branches found in this study are indicated in green and
894   the currents coming from the north/south are in blue/orange. The width of the current arrows is
895   proportional to the current amplitude and the dotted arrows represent the currents with the
896   minimum amplitudes. C1 and C2 are for respectively, the cyclonic circulations highlighted
897   between 44°-50° W and 35°-45° W.

898

899

900

901

902

903

904

905

906

907

908

909

910

911
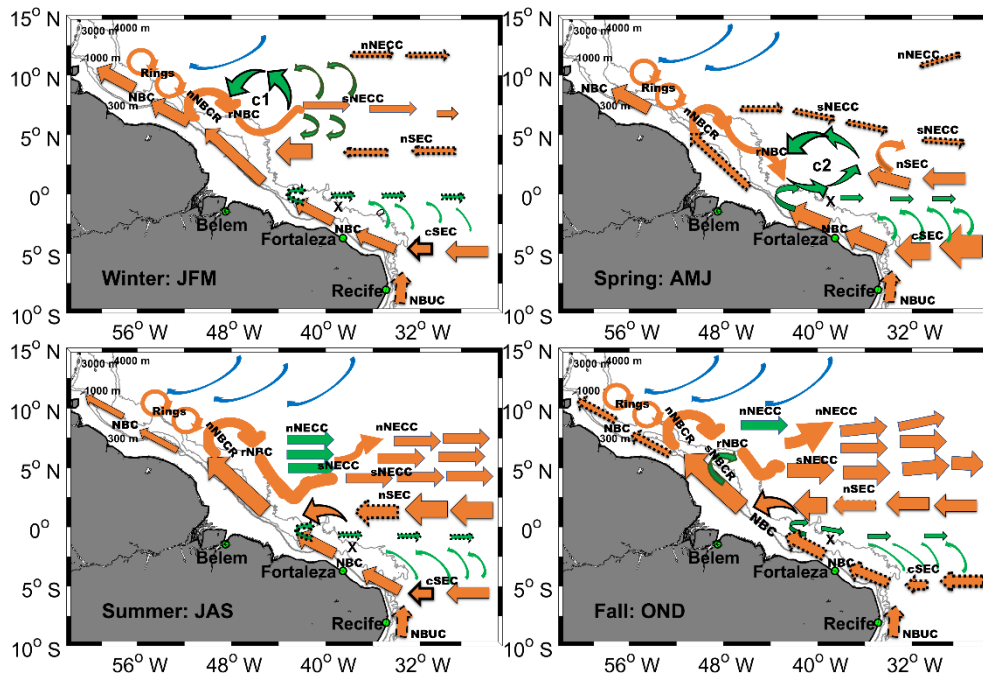
Figure 9~~10~~. Schematic view of the seasonal maps of the tropical western boundary circulation. C1 and C2 represent the cyclonic circulations highlighted in this study. The wider (dotted thin) arrows show current branches with maximum (minimum) intensity. The subsurface NBUC is represented by dashed arrows. The already known current branches are in orange/blue. The green arrows characterize the new branches observed. NBC is the North Brazil Current; nNBCR and sNBCR are the northern and the southern flows of the North Brazil Current retroflection, respectively; rNBC is the retroflected branch of North Brazil current; nNECC and sNECC are the northern and the southern branches of the North Equatorial Countercurrent (NECC), respectively; cSEC and nSEC are the central and the northern branches of the South Equatorial Current (SEC), respectively.

931 Concerning the interannual variability, Hormann et al. (2012), based on the analyses of 17 year
932 of altimetry and drifter' data, found interesting scenarios about the NECC spatial and temporal
933 variability. However, they did not separate the sNECC from the nNECC. In their study, the
934 authors have associated the strengthening of the NECC in the whole basin to the negative phase
935 of the AZM, and its northward shift to the positive phase of the AMM. Our results show
936 different behaviors of the NECC system as a function of the branch and core location. We also
937 showed possible relationships between the southern NECC branch intensity and location with
938 the AMM phases at 42° W, and conversely a possible relationship between the southern NECC
939 branch intensity and location with the AZM phases at 32° W. These results open the way to
940 deeper investigations in future studies.

941 **7   Summary and Perspectives**

942 Twenty-five years (1993-2017) of gridded altimetry data from CMEMS were used to improve
943 the description of the seasonal and interannual variations of the western boundary circulation
944 of the tropical Atlantic. To do so, a new approach based on the calculation of the current
945 intensity was applied to~~Therefore, we defined~~ six horizontal sections defined. These sections
946 have been designed to intersect~~crossing~~ the path of the principal~~main~~ upper ocean flows over
947 the west tropical Atlantic~~layer currents' veins~~. Copernicus Climate Service~~C3S~~ ERA5 wind
948 estimates and the NOAA OI SST v2 product were also used to investigate the possible link
949 between the variability of the regional circulation and the large-scale remote wind forcing on
950 one hand, and the tropical Atlantic climate modes on the other hand.

951 Our results highlight a complex regional circulation, with significant seasonal and year-to-year
952 variations of the current's^2 intensity and location. South of the equator, we observe a
953 stronger/weaker central branch of the South Equatorial Atlantic (cSEC) and of the North Brazil
954 Current (NBC) during boreal spring/fall. North of the equator, the NBC component flowing
955 along the Guyana coast exhibits a similar annual cycle. However, between both, the NBC part
956 located before the retroflection is out of phase (i.e. stronger during summer-fall), when fed by
957 the northern branch of the South Equatorial Current (nSEC). Its larger amplitudes appear during
958 boreal fall, 3-4 months after the maximum of the remote wind stress curl (WSC) strength (in
959 August). The North Equatorial Countercurrent (NECC) is connected with the retroflected
960 branch of the NBC, and both show similar annual cycle. A secondary North Brazil Current
961 Retroflection (NBCR) was observed for the first time during boreal fall in this study: it is
962 located between 4°-6° N. The two-core/branch structure of the NECC during the second half of

the year was also confirmed and analyzed separately. Between 0°-5° N and 35°-45° W, a surface cyclonic circulation develops during boreal spring. It is found to initiate the growth of the NECC at 42° W in June. However, at 32° W, the NECC doesn't show any connection with this cyclonic circulation, but starts its seasonal cycle earlier in April when the ITCZ migrates northward and the remote WSC strengthens. In the equatorial region, between 2° S-2° N, the geostrophic currents show the presence of an equatorial surface eastward flow which has a seasonal cycle similar to the Equatorial Undercurrent (EUC). But the near-surface Ekman currents have to be taken into account here to have a good description of the surface circulation.

Concerning the interannual variability, it is much weaker than the seasonal one. We do not observe an obvious picture at regional scale but it is more important in the eastern part of the basin. The analysis of the changes in characteristics of the different current branches (intensity and core location), with respect to the tropical Atlantic climate modes, shows different possible scenarios associated with one or both modes. It opens the way to further investigations concerning the link between the Atlantic climate modes (ACM) and the current transports, not possible with altimetry alone.

As a conclusion, this study demonstrates the ability of altimetry to characterize the seasonal and interannual variability of the surface circulation in the study area. It confirms previous findings but also significantly complements the knowledge of the different currents at regional scale. Combined use of regional modelling, altimetry and in-situ observations will allow us to go further in the understanding of the spatial and temporal structure of the regional circulation. The intraseasonal variability, significant in the near-shore region of the study area (Fig. 2d) is not studied here. It will be the subject of a future work, based on a coastal altimetry product that will allow a significantly better resolution and accuracy along the continental shelf, compared to a gridded product.

Authors contribution

Djoirka M. Dimoune performed the data analyses as part of his PhD thesis. Florence Birol, Fabrice Hernandez, Fabien Leger and Moacyr Araujo supervised this research.

Competing interests

The authors declare that they have no conflict of interest.

Acknowledgements

This work has been supported by: CAPES Foundation who funded the thesis of the first author, CAPES-Print (grants 88887.467360/2019-00) who funded his visit to LEGOS during the first six months spent in the laboratory, and LEGOS and the CNES/TOSCA program as part of SWOT-Brésil project that funded the three last months of extension in the laboratory. The authors thank the CMEMS, who processed the geostrophic currents data and made them available. They thank also the ECMWF and NOAA respectively who made available the mean wind fields data and SST for the work. Thank also the two reviewers of this paper for their helpful suggestions and corrections which helped to improve and make this work more understandable Thanks also to Joël Sudre from LEGOS who developped the GEKCO product used for this study. This work represents collaboration by the INCT AmbTropic, the Brazilian National Institute of Science and Technology for Tropical Marine Environments, CNPq/FAPESB (grants 565054/2010-4 and 8936/2011 and 465634/2014-1) and the Brazilian Research Network on Global Climate Change FINEP/Rede CLIMA (grants 01.13.0353-00). This is also a contribution to the LMI-TAPIOCA and to the TRIATLAS project, which has received funding from the European Union's Horizon 2020 research and innovation program under grant agreement No 817578

References

Aguedjou, H. M. A., Dadou, I., Chaigneau, A., Morel, Y., and Alory, G.: Eddies in the Tropical Atlantic Ocean and their seasonal variability, Geophys. Res. Lett., *46*(21), 12156-12164, https://doi.org/10.1029/2019GL083925, 2019.

Araujo, M., Noriega, C., Hounsou-Gbo, G. A., Veleda, D., Araujo, J., Bruto, L., Feitosa, F., Flores-Montes, M., Lefèvre, N., Melo, P., Ostuska, A., Travassos, K., Schwamborn, R., Neumann-Leitão, S.: A synoptic assessment of the amazon river-ocean continuum during boreal autumn: From physics to plankton communities and carbon flux, Front. Microbiol., 8, 1358, https://doi.org/10.3389/fmicb.2017.01358, 2017.

Arbic, B. K., Scott, R. B., Chelton, D. B., Richman, J. G., and Shriver, J. F.: Effects of stencil width on surface ocean geostrophic velocity and vorticity estimation from gridded satellite altimeter data, J. Geophys. Res.-Oceans, 117(C3), https://doi.org/10.1029/2011jc007367, 2012.

1022 Aroucha, L. C., Veleda, D., Lopes, F. S., Tyaquiçã, P., Lefèvre, N., and Araujo, M.: Intra-and
1023 Inter-Annual Variability of North Brazil Current Rings Using Angular Momentum Eddy
1024 Detection and Tracking Algorithm: Observations From 1993 to 2016, J. Geophys. Res.-
1025 Oceans, 125(12), e2019JC015921, https://doi.org/10.1029/2019jc015921, 2020.

1026 Burmeister K., Lübbecke, J. F.,Brandt, P., and Duteil, O.: Interannual variability of the
1027 Atlantic North Equatorial Undercurrent and its impact on oxygen, J. Geophys. Res.-Oceans,
1028 124, 2348–2373, https://doi.org/10.1029/2018JC014760, 2019.

1029 Bourles, B., Molinari, R. L., Johns, E., Wilson, W. D., and Leaman, K. D.: Upper layer
1030 currents in the western tropical North Atlantic (1989–1991), J. Geophys. Res.-Oceans,
1031 104(C1), 1361-1375, https://doi.org/10.1029/1998jc9000250, 1999.

1032 Bourlès, B., Gouriou, Y., and Chuchla, R.: On the circulation in the upper layer of the western
1033 equatorial Atlantic, J. Geophys. Res.-Oceans, 104(C9), 21151-21170,
1034 https://doi.org/10.1029/1999jc900058, 1999.

1035 Brandt, P., Schott, F. A., Provost, C., Kartavtseff, A., Hormann, V., Bourlès, B., and Fischer,
1036 J.: Circulation in the central equatorial Atlantic: Mean and intraseasonal to seasonal
1037 variability, Geophys. Res. Lett., 33(7), https://doi.org/10.1029/2005gl025498, 2006.

1038 Brandt, P., Claus, M., Greatbatch, R. J., Kopte, R., Toole, J. M., Johns, W. E., and Böning, C.
1039 W.: Annual and semiannual cycle of equatorial Atlantic circulation associated with basin-
1040 mode resonance, J. Phys. Oceanogr., 46(10), 3011-3029, https://doi.org/10.1175/jpo-d-15-
1041 0248.1, 2016.

1042 Cabos, W., de la Vara, A., and Koseki, S.: Tropical Atlantic variability: observations and
1043 modelling, Atmosphere, 10(9), 502, https://doi.org/10.3390/atmos10090502, 2019.

1044 Cochrane, J. D., Kelly Jr, F. J., and Olling, C. R.: Subthermocline countercurrents in the
1045 western equatorial Atlantic Ocean, J. Phys. Oceanogr., 9(4), 724-738,
1046 https://doi.org/10.1175/1520-0485(1979)009<0724:scitwe>2.0.co;2, 1979.

1047 Didden, N., and Schott, F.: Seasonal variations in the western tropical Atlantic: Surface
1048 circulation from Geosat altimetry and WOCE model results, J. Geophys. Res.-Oceans,
1049 97(C3), 3529-3541, https://doi.org/10.1029/91jc02860, 1992.

1050 Dossa, A. N., Silva, A. C., Chaigneau, A., Eldin, G., Araujo, M., and Bertrand, A.: Near-
1051 surface western boundary circulation off Northeast Brazil, Prog. Oceanogr., 190, 102475,
1052 https://doi.org/10.1016/j.pocean.2020.102475, 2021.

1053 Ffield, A.: North Brazil current rings viewed by TRMM Microwave Imager SST and the
1054 influence of the Amazon Plume, Deep-Sea Res. Pt. I, 52(1), 137-160,
1055 https://doi.org/10.1016/j.dsr.2004.05.013, 2005.

1056 Fonseca, C. A., Goni, G. J., Johns, W. E., and Campos, E. J.: Investigation of the north Brazil
1057 current retroflection and north equatorial countercurrent variability, Geophys. Res. Lett.,
1058 31(21), https://doi.org/10.1029/2004gl020054, 2004.

1059 Fratantoni, D. M., Johns, W. E., Townsend, T. L., and Hurlburt, H. E.: Low-latitude
1060 circulation and mass transport pathways in a model of the tropical Atlantic Ocean, J. Phys.
1061 Oceanogr., 30(8), 1944-1966,
1062 https://doi.org/10.1175/15200485(2000)030<1944:LLCAMT>2.0.CO;2, 2000.

1063 Garzoli, S. L., and Katz, E. J.: The forced annual reversal of the Atlantic North Equatorial
1064 Countercurrent, J. Phys. Oceanogr., 13(11), 2082-2090, https://doi.org/10.1175/1520-
1065 0485(1983)013<2082:tfarot>2.0.co;2, 1983.

1066 Garzoli, S. L.: The Atlantic North Equatorial Countercurrent: Models and observations, J.
1067 Geophys. Res.-Oceans, 97 (C11), 17931-17946, https://doi.org/10.1029/92jc01363, 1992.

1068 Garzoli, S. L., Ffield, A., and Yao, Q.: North Brazil Current rings and the variability in the
1069 latitude of retroflection, Elsevier Oceanogr. Ser., 68, 357-373, https://doi.org/10.1016/s0422-
1070 9894(03)80154-x, 2003.

1071 Garzoli, S. L., Ffield, A., Johns, W. E., and Yao, Q.: North Brazil Current retroflection and
1072 transports, J. Geophys. Res.-Oceans, 109(C1), https://doi.org/10.1029/2003jc001775, 2004.

1073 Garzoli, S. L., and Matano, R.: The South Atlantic and the Atlantic meridional overturning
1074 circulation, Deep-Sea Res. II, 58(17-18), 1837-1847,
1075 https://doi.org/10.1016/j.dsr2.2010.10.063, 2011.

1076 Gill, A. E., and Adrian, E.: Atmosphere-ocean dynamics, Vol. 30, Academic press,
1077 https://doi.org/10.1016/s0074-6142(08)60025-x, 1982.

Góes, M., and Wainer, I.: Equatorial currents transport changes for extreme warm and cold events in the Atlantic Ocean, Geophys. Res. Lett., 30(5), https://doi.org/10.1029/2002gl015707, 2003.

Goes, M., Molinari, R., da Silveira, I., and Wainer, I.: Retroflections of the north brazil current during february 2002, Deep-Sea Res. Pt. I, *52*(4), 647-667, https://doi.org/10.1016/j.dsr.2004.10.010, 2005.

Goni, G. J., and Johns, W. E.: Synoptic study of warm rings in the North Brazil Current retroflection region using satellite altimetry, Elsevier Oceanogr. Ser., 68, 335-356, https://doi.org/10.1016/s0422-9894(03)80153-8, 2003.

Hazeleger, W., and De Vries, P.: Fate of the Equatorial Undercurrent in the Atlantic, Elsevier Oceanogr. Ser., 68, 175-191, https://doi.org/10.1016/s0422-9894(03)80146-0, 2003.

Hazeleger, W., de Vries, P., and Friocourt, Y.: Sources of the Equatorial Undercurrent in the Atlantic in a high-resolution ocean model, J. Phys. Oceanogr., 33(4), 677-693, https://doi.org/10.1175/1520-0485(2003)33<677:soteui>2.0.co;2, 2003.

Hisard, P., and Hénin, C.: Response of the equatorial Atlantic Ocean to the 1983–1984 wind from the Programme Français Océan et Climat dans l'Atlantique Equatorial cruise data set, J. Geophys. Res.-Oceans, 92(C4), 3759-3768, https://doi.org/10.1029/jc092ic04p03759, 1987.

Hormann, V., and Brandt, P.: Atlantic Equatorial Undercurrent and associated cold tongue variability, J. Geophys. Res.-Oceans, 112(C6), https://doi.org/10.1029/2006jc003931, 2007.

Hormann, V., Lumpkin, R., and Foltz, G. R.: Interannual North Equatorial Countercurrent variability and its relation to tropical Atlantic climate modes, J. Geophys. Res.-Oceans, 117(C4), https://doi.org/10.1029/2011jc007697, 2012.

Jochum, M., and Malanotte-Rizzoli, P.: On the generation of North Brazil Current rings, J. Mar. Res., 61(2), 147-173, https://doi.org/10.1357/002224003322005050, 2003.

Johns, W. E., Lee, T. N., Schott, F. A., Zantopp, R. J., and Evans, R. H.: The North Brazil Current retroflection: Seasonal structure and eddy variability, J. Geophys. Res.-Oceans, 95(C12), 22103-22120, https://doi.org/10.1029/jc095ic12p22103, 1990.

Johns, W. E., Lee, T. N., Beardsley, R. C., Candela, J., Limeburner, R., and Castro, B.: Annual cycle and variability of the North Brazil Current, J. Phys. Oceanogr., *28*(1), 103-128, https://doi.org/10.1175/1520-0485(1998)028<0103:acavot>2.0.co;2, 1998.

1108   Lagerloef, G. S., Mitchum, G. T., Lukas, R. B., and Niiler, P. P.: Tropical Pacific near-surface

1109   currents estimated from altimeter, wind, and drifter data, J. Geophys. Res.-Oceans, 104(C10),

1110   23313-23326, https://doi.org/10.1029/1999jc900197, 1999.

1111   Large, W. G., and Pond, S.: Open ocean momentum flux measurements in moderate to strong

1112   winds, J. Phys. Oceanogr., 11(3), 324-336, https://doi.org/10.1175/1520-

1113   0485(1981)011<0324:oomfmi>2.0.co;2, 1981.

1114   NRSC: OSCAT Wind stress and Wind stress curl products, Ocean Sciences Group, Earth and

1115   Climate Science Area, Hyderabad, India, 18 pp., 2013.

1116   Peterson, R. G., and Stramma, L.: Upper-level circulation in the South Atlantic Ocean, Prog.

1117   Oceanogr., 26(1), 1-73, https://doi.org/10.1016/0079-6611(91)90006-8, 1991.

1118   Provost, C., Arnault, S., Chouaib, N., Kartavtseff, A., Bunge, L., and Sultan, E.:

1119   TOPEX/Poseidon and Jason equatorial sea surface slope anomaly in the Atlantic in 2002:

1120   Comparison with wind and current measurements at 23W, Mar. Geod., 27(1-2), 31-45,

1121   https://doi.org/10.1080/01490410490465274, 2004.

1122   Pujol, M. I., Faugère, Y., Taburet, G., Dupuy, S., Pelloquin, C., Ablain, M., and Picot, N.:

1123   DUACS DT2014: the new multi-mission altimeter data set reprocessed over 20 years, Ocean

1124   Sci., 12(5), 1067-1090, https://doi.org/10.5194/os-2015-110, 2016.

1125   Richardson, P. L., and Walsh, D.: Mapping climatological seasonal variations of surface

1126   currents in the tropical Atlantic using ship drifts, J. Geophys. Res.-Oceans, 91(C9), 10537-

1127   10550, https://doi.org/10.1029/jc091ic09p10537, 1986.

1128   Rodrigues, R. R., Rothstein, L. M., and Wimbush, M.: Seasonal variability of the South

1129   Equatorial Current bifurcation in the Atlantic Ocean: A numerical study, J. Phys. Oceanogr.,

1130   37(1), 16-30, https://doi.org/10.1175/jpo2983.1, 2007.

1131   Schmitz Jr, W. J., and McCartney, M. S.: On the north Atlantic circulation, Rev. Geophys.,

1132   31(1), 29-49, https://doi.org/10.1029/92RG02583, 1993.

1133   Schott, F. A., Stramma, L., and Fischer, J.: The warm water inflow into the western tropical

1134   Atlantic boundary regime, spring 1994, J. Geophys. Res.-Oceans, 100(C12), 24745-24760,

1135   https://doi.org/10.1029/95jc02803, 1995.

Schott, F. A., Fischer, J., and Stramma, L.: Transports and pathways of the upper-layer circulation in the western tropical Atlantic, J. Phys. Oceanogr., 28(10), 1904-1928, https://doi.org/10.1175/1520-0485(1998)028<1904:tapotu>2.0.co;2, 1998.

Schott, F. A., McCreary Jr, J. P., and Johnson, G. C.: Shallow overturning circulations of the tropical-subtropical oceans, Washington DC American Geophysical Union Geophys. Monogr. Ser., 147, 261-304, https://doi.org/10.1029/147gm15, 2004.

Servain, J.: Simple climatic indices for the tropical Atlantic Ocean and some applications, J. Geophys. Res.-Oceans, 96 (C8), 15137-15146, https://doi.org/10.1029/91jc01046, 1991.

Silva, M., Araujo, M., Servain, J., Penven, P., and Lentini, C. A.: High-resolution regional ocean dynamics simulation in the southwestern tropical Atlantic. Ocean Model., 30(4), 256-269, https://doi.org/10.1016/j.ocemod.2009.07.002, 2009.

Stramma, L., and Schott, F.: The mean flow field of the tropical Atlantic Ocean, Deep-Sea Res. Pt. II, 46(1-2), 279-303, https://doi.org/10.1016/s0967-0645(98)00109-x, 1999.

Stramma, L., and England, M.: On the water masses and mean circulation of the South Atlantic Ocean, J. Geophys. Res.-Oceans, 104(C9), 20863-20883, https://doi.org/10.1029/1999JC900139, 1999.

Sudre, J., Maes, C., and Garçon, V.: On the global estimates of geostrophic and Ekman surface currents, Limnol. Oceanogr.: Fluids Environ., 3(1), 1-20, https://doi.org/10.1215/21573689-2071927, 2013.

Trenberth, K. E., Large, W. G., and Olson, J. G.: The mean annual cycle in global ocean wind stress, J. Phys. Oceanogr., 20(11), 1742-1760, https://doi.org/10.1175/1520-0485(1990)020<1742:TMACIG>2.0.CO;2, 1990.

Tuchen, F. P., Lübbecke, J. F., Schmidtko, S., Hummels, R., and Böning, C. W. : The Atlantic subtropical cells inferred from observations, J. Geophys. Res.-Oceans, *124*(11), 7591-7605, https://doi.org/10.1029/2019JC015396, 2019.

Tuchen, F. P., Lübbecke, J. F., Brandt, P., and Fu, Y.: Observed transport variability of the Atlantic Subtropical Cells and their connection to tropical sea surface temperature variability. J. Geophys. Res.-Oceans, *125*(12), e2020JC016592, https://doi.org/10.1029/2020JC016592, 2020.

Tuchen, F.P., Brandt, P., Lübbecke, J. F., and Hummels, R.: Transports and Pathways of the Tropical AMOC Return Flow From Argo Data and Shipboard Velocity Measurements. J. Geophys. Res.-Oceans, 127 (2), e2021JC018115, https://doi.org/10.1029/2021JC018115, 2022.

Urbano, D. F., Jochum, M., and Da Silveira, I. C. A.: Rediscovering the second core of the Atlantic NECC, Ocean model., 12(1-2), 1-15, https://doi.org/10.1016/j.ocemod.2005.04.003, 2006.

Urbano, D. F., De Almeida, R. A. F., and Nobre, P.: Equatorial Undercurrent and North Equatorial Countercurrent at 38 W: A new perspective from direct velocity data, J. Geophys. Res.-Oceans, 113(C4), https://doi.org/10.1029/2007jc004215, 2008.

Verdy, A., and Jochum, M.: A note on the validity of the Sverdrup balance in the Atlantic North Equatorial Countercurrent, Deep-Sea Res. Pt. I, 52(1), 179-188, https://doi.org/10.1016/j.dsr.2004.05.014, 2005.

Zebiak, S. E.: Air–Sea Interaction in the Equatorial Atlantic Region, J. Clim., 6 (8), 1567-1586, https://doi.org/10.1175/1520-0442(1993)006<1567:AIITEA>2.0.CO;2, 1993.

Zheng, Y., and Giese, B. S.: Ocean heat transport in simple ocean data assimilation: Structure and mechanisms, J. Geophys. Res.-Oceans, 114(C11), https://doi.org/10.1029/2008jc005190, 2009.